Two-stage exhumation of subducted Saxothuringian continental crust records underplating in the subduction channel and collisional forced folding (Krkonoše-Jizera Mts., Bohemian Massif)

Petr JEŘÁBEK[a,b*], Jiří KONOPÁSEK[c,b], Eliška ŽÁČKOVÁ[b]

[a] Institute of Petrology and Structural Geology, Faculty of Science, Charles University in Prague, Albertov 6, 128 43 Prague, Czech Republic, email: jerabek.petr@natur.cuni.cz, phone: +420 221951534

[b] Czech Geological Survey, Klárov 3, 118 21 Prague, Czech Republic

[c] Department of Geology, University of Tromsø, Dramsveien 201, 9037, Tromsø, Norway

Key words: exhumation of high-pressure rocks; quartz deformation microstructures and textures; phase equilibrium modelling; Saxothuringian domain; West Sudetes; Bohemian Massif

Abstract

The Krkonoše-Jizera Massif in the northern part of the Variscan Bohemian Massif provides insight into the exhumation mechanisms for subducted continental crust. The studied region exposes a relatively large portion of a flat-lying subduction-related complex that extends approximately 50 kilometres away from the paleosuture. wide extent of HP-LT metamorphism has been confirmed by new P-T estimates indicating temperatures of 400–450°C at 14–16 kbar and 450–520°C at 14–18 kbar for the easternmost and westernmost parts of the studied area, respectively. A detailed study of metamorphic assemblages associated with individual deformation fabrics together with analysis of quartz deformation microstructures and textures allowed characterisation of the observed deformation structures in terms of their subduction-exhumation memory. An integration of the lithostratigraphic, metamorphic and structural data documents a subduction of distal and proximal parts of the Saxothuringian passive margin to high-pressure conditions and their subsequent exhumation during two distinct stages. The initial stage of exhumation has an adiabatic character interpreted as the buoyancy driven return of continental material from the subduction channel resulting in underplating and progressive nappe stacking at the base of the Teplá-Barrandian upper plate. With the transition from continental subduction to continental collision during later stages of the convergence, the underplated high-pressure rocks were further exhumed due to shortening in the accretionary wedge. This shortening is associated with the formation of large-scale recumbent forced folds extending across the entire studied area.

1. Introduction

Fossil subduction interfaces (paleo-sutures) convey significant information on the dynamics of subduction and exhumation processes (Platt, 1993; Chemenda et al., 1995; Jolivet et al., 2003; Agard and Vitale-Brovarone, 2013; Hacker and Gerya, 2013; Burov et al., 2014). The subduction channels are defined as tabular or wedge-like areas of variable size, internal structure and compositional form between the upper and lower plates during slab subduction. These zones experience complex physical and chemical interactions and they are typically marked by exhumed portions of previously subducted material (Hsu, 1971; Cloos, 1982). Recent studies aiming to decipher the architecture of fossil subduction zones are thus inevitably linked to detailed petrology (e.g. Hacker et al., 2003; Konopásek and Schulmann, 2005; Agard et al., 2010; Plunder et al., 2013, 2015; Philippon et al., 2013; Lopéz-Carmona et al., 2014). At the same time, proper characterisation of the deformational record in subduction channels is complicated by identical kinematic boundary conditions and parallelism of both subduction and exhumation fabrics. Only a few studies have described deformation structures in association with particular mineral assemblages enabling deformation processes to be linked with specific parts/levels of the channel (e.g. Plunder et al., 2012; 2013; Hyppolito et al., 2015; Keppler et al., 2016). In addition, large-scale forced folds associated with major detachment surfaces have been repeatedly reported from fossil subduction interfaces (Searle et al., 2004; Agard et al., 2010; Plunder et al., 2013; Xypolias and Alsop, 2014). On the other hand, the identification and reconstruction of mega- to crustal-scale fold structures in such settings is generally impossible without complementary information based on metamorphic petrology and/or deformation microstructures (cf. Konopásek et al., 2001; Štípská et al., 2004; Jeřábek et al., 2008; Skrzypek et al., 2011; Morales et al., 2011).

The Saxothuringian domain in the NW part of the Bohemian Massif represents a passive margin of the Saxothuringian/Rheic Ocean that opened in Cambrian–Ordovician and was subducted beneath the easterly core of the Bohemian Massif during Devonian–Carboniferous Variscan orogeny (e.g. Matte et al., 1990; Franke, 2000; Schulmann et al., 2009). The current exposure of the NE-SW trending paleo-suture, identified between the lower plate Saxothuringian and the upper plate Teplá-Barrandian domains, reveals along-strike variations in metamorphic conditions of subducted continental crust marked by HP–UHP/MT–HT metamorphism in the SW Erzgebirge Mts. and by HP/LT metamorphism in the NE West Sudetes (e.g. Cháb and Vrána, 1979; Guiraud and Burg, 1984; Kryza et al., 1990; Schmädicke et al., 1992; Smulikowski, 1995; Patočka et al., 1996; Rötzler et al., 1998; Konopásek, 1998; 2001; Nasdala and Massonne, 2000; Žáčková et al., 2010; Kotková et al., 2011; Faryad and Kachlík, 2013).

This work provides a detailed documentation of the tectono-metamorphic record in the subduction-accretionary complex of the Krkonoše-Jizera Massif in the West Sudetes. The subduction-related evolution of this region is interpreted via a multidisciplinary approach combining the results of field structural geology and quartz deformation microstructures and textures with petrography and phase equilibrium modelling. This approach allowed us to identify an imbricated stack of high-pressure slices derived from the lower plate (the Saxothuringian passive margin) which experienced two-stage exhumation accommodated by two contrasting mechanisms.

2. Geological setting

The northeastern part of the Saxothuringian domain in the Variscan orogenic belt of Central Europe is represented by the West Sudetes at the northern margin of the Bohemian Massif (Fig.1a; Franke et al., 1993; Narębski, 1994; Franke and Żelaźniewicz, 2000). The Krkonoše-Jizera Massif is one of several lithotectonic units defined in this area and it has been interpreted as a Variscan subduction-accretionary complex related to southeastward subduction and underthrusting of the Saxothuringian plate (Kachlík and Patočka, 1998; Mazur et al., 2006) below the Teplá-Barrandian domain (Mazur and Aleksandrowski, 2001). In its core, the Krkonoše-Jizera Massif (Fig. 1b) comprises a large body of Upper Cambrian/Lower Ordovician orthogneiss (Borkowska et al., 1980; Korytowski et al., 1993; Oliver et al., 1993; Kröner et al., 2001). The gneissic core is surrounded by metamorphosed volcano-sedimentary rocks of the Saxothuringian passive margin, deposited during the Early Palaeozoic intracontinental rifting of the Cadomian basement and subsequent development of an oceanic basin (Kryza et al., 1995; 2007; Winchester et al.; 1995; 2003; Kachlík and Patočka, 1998; Patočka et al., 2000; Dostál et al., 2001; Žáčková et al., 2012). The subduction and orogenic period in the West Sudetes is marked by high-pressure metamorphism of the Early Palaeozoic passive margin deposits (Cháb and Vrána, 1979; Guiraud and Burg, 1984; Kryza et al., 1990; Smulikowski, 1995; Patočka et al., 1996, Žáčková et al., 2010), associated nappe stacking, exhumation and post-metamorphic folding of the entire metamorphic complex (Mazur, 1995; Mazur and Kryza, 1996; Seston et al., 2000; Mazur and Aleksandrowski, 2001; Žáčková et al., 2010). The central part of the Krkonoše-Jizera Massif was at the late stages of the Variscan orogeny, between ~320 and ~315 Ma, intruded by the multistage Krkonoše-Jizera granite plutonic complex (Machowiak and Armstrong, 2007; Žák et al., 2013).

The current configuration of rock complexes in the West Sudetes has been attributed to the nappe tectonics identified on the basis of geochemical, geochronological, structural and metamorphic data (Seston et al., 2000; Mazur and Aleksandrowski, 2001). The original nappe division was recently revised by Žáčková et al. (2010) who proposed a distinction of four major tectonic units. The par-autochthonous unit (i) is represented by Neoproterozoic to Upper Cambrian/Lower Ordovician (meta)granitoids (Kröner et al., 1994; Tichomirowa et al., 2001) of the Lusatian and Jizera Massifs (Fig. 1a) with very low-grade Neoproterozoic–Lower Palaeozoic cover (the Ještěd Unit; Chaloupský, 1989; Chlupáč, 1993; Kachlík and Kozdrój, 2001). The lower thrust sheet (ii) is exposed structurally above the Jizera orthogneiss in the southeastern part of the Krkonoše-Jizera Massif and comprises mostly ± garnet-bearing micaschists with subordinate bodies of orthogneisses, quartzites, calcsilicate rocks and marbles (Fig. 1b). A petrological study of garnet-bearing samples suggested blueschist-facies metamorphism in the range of 18–19 kbar and 460–520°C (Žáčková et al., 2010). A thick orthogneiss body with a U-shape map section is situated close to the contact of the lower and middle thrust sheet (Fig. 1b). The middle thrust sheet (iii) is formed by garnet-free micaschists, phyllites and marbles with a high proportion of metavolcanics (Fig. 1b). The metabasites of this unit show blueschist-facies metamorphism, which reached conditions of 300–530°C and 6.5–12 kbar (Cháb and Vrána, 1979; Guiraud and Burg, 1984; Kryza and Mazur, 1995; Smulikowski, 1995; Patočka et al., 1996). The uppermost thrust sheet (iv) is the Leszczyniec Unit (Fig. 1a) dominated by metabasites with low intensity of deformation and medium pressure metamorphism (Kryza and Mazur, 1995; Seston et al., 2000).

For the purpose of this article the studied area covering the lower and middle thrust sheets can be divided into several belts with distinct lithological content (Figs. 1b and 2): (1) garnet-bearing micaschist, (2) orthogneiss, (3) garnet-free micaschist, phyllite and metavolcanics, and (4) metabasite. Garnetiferous micaschists (1) with locally preserved chloritoid inclusions in the core of garnet porphyroblasts document an early high-pressure metamorphic event (Žáčková et al., 2010). Garnet-free (3), as well as garnet-bearing (1) micaschists were affected by widespread blastesis of albite, which has been associated with decompression from the HP-stage and release of sodium from the deforming orthogneiss (Žáčková et al., 2010). The chloritoid-bearing and albite-free phyllites (3) are characterised in detail in this study and two samples (collected from the areas of the Rýchory Mts. and Železný Brod see Fig. 1b) were used for P-T estimates. Orthogneisses (2) appear either as an equigranular variety or as typical augen orthogneiss. The link between their metamorphism and observed deformation fabrics from the microstructural point of view is discussed in this study. The metabasites (4) are usually greenschists with relics of blueschist-facies metamorphism (Cháb and Vrána, 1979; Guiraud and Burg, 1984; Patočka et al., 1996).

3. Succession of deformation structures

Our structural analysis revealed that the overall structure of the southern Krkonoše-Jizera

Massif can be interpreted as tens of kilometers-scale isoclinal folds with generally east-dipping axial plane, two hinge zones and three principal limbs occupying the entire map view (Fig. 2). A recognition of this large-scale structure has been hindered by 1) a complicated shape of the isoclinal folds and 2) subsequent re-folding resulting in a complex final geometry of interfering folds (Fig. 2a). The reconstruction of the folds is based on our extensive structural dataset consisting of ~1250 documented outcrops and ~3500 structural measurements collected during 1:25 000 scale geological mapping by the Czech Geological Survey. For the sake of clarity in the following text, the presumed shape of the folds is revealed here so that the studied area can be divided into three regions corresponding to the spatial extent of the three principal limbs of the two isoclinal mega-folds. Limb 1 is the uppermost and occupies eastern part of the studied area, Limb 2 is situated in the middle and represents the central part of the studied area and Limb 3 is the lowermost and crops out in the west (cf. Figs. 1b and 2b). Four deformation fabrics/events have been recognized in the studied area.

3.1. D1 deformation

The oldest deformation fabric S1 is preserved as relics namely in the hinge zones of isoclinal F2 folds (Fig. 3a–e) due to the subsequent intense overprint of F2 limbs by axial planar cleavage S2. S1 in the F2 limbs can be identified when present as distinct compositional layering parallel to S1 in calc-silicates, metacarbonates and metabasites/metavolcanites of the southern Krkonoše-Jizera Massif. However, in micaschists, quartzites and orthogneisses the distinction between parallel S1 and S2 in the F2 limbs is nearly impossible. The large-scale hinge zone of the F2 mega-fold, defined by an E–W trending and steeply-dipping portion of the orthogneiss body (cf. hinge 1 in Fig. 2b and Figs. 4 and 5a: 3), preserves the least overprinted S1 fabric. In the metabasites and metavolcanites in the east and west of the studied area (Rýchory Mountains and Železný Brod, respectively; Fig 1b), S1 is defined by compositional layering marked by alternation of epidote-rich, sodic amphibole and/or plagioclase-rich layers (Fig. 3a) developed during blueschist-facies metamorphism (Cháb and Vrána, 1979; Guiraud and

Burg, 1984; Patočka et al., 1996).

3.2. D2 deformation

The D2 event is associated with the development of small to mega-scale recumbent isoclinal folds F2 and formation of penetrative greenschist-facies metamorphic foliation S2, which reworks S1 in the limbs of the F2 folds and is axial planar in their hinges. The S2 overprinting S1 (S2/S1), which are macroscopically indistinguishable in the F2 limbs, is thus the dominant fabric in the entire region (Fig. 4). In metasediments and metabasites, the metamorphic foliation mainly corresponds to the axial planar cleavage S2 (Fig. 3c–e) while in orthogneiss the S1 foliation is apparently well preserved in the hinge of the F2 megafold (hinge 1 in Fig. 2b) and is reworked to a variable extent by S2 in F2 limbs. Due to similar microscopic appearance, the distinction of S1 and S2 in F2 limbs is only possible on the basis of differences in texture (CPO) and metamorphic record (see below). In the metasediments, S2 is associated with the widespread occurrence of albite porphyroblasts showing syn- to mostly post-kinematic relations with respect to the S2/S1 foliation (cf. Fig. 3d, e, g). In places, where S2/S1 was not reoriented by subsequent upright folding D3 (e.g. 7–8 in Fig. 5a), the S1/S2 fabric is subvertical to steeply eastward dipping in the eastern Limb 1 (1–2 in Fig. 5a) and becomes gently eastward dipping to subhorizontal towards the west in Limbs 2 and 3 (Figs. 4 and 5a: 5–7). S2/S1 bears mineral and stretching lineation, which generally plunges towards ESE (Figs. 4 and 5b). The stretching lineation is best preserved in the orthogneiss, where it is defined by shape preferred orientation of recrystallised quartz and feldspar aggregates. Again, the stretching lineation L1 and L2 in the orthogneiss are difficult to distinguish, however their orientation in the S1- and S2-dominated regions indicates that both lineations are parallel. In the metasediments, the mineral lineation defined by micas is in most cases obliterated by subsequent crenulation lineation FA3 (Fig. 3h). Fold axes of macroscopic isoclinal folds F2 show a distinct spatial arrangement across the studied area (Fig. 5b, crosses in the pole figures). In the vicinity of the U-shape orthogneiss body in the east (Limb 1 and hinge 1; Figs. 1b and 2b), the axes of F2 isoclinal folds are parallel to the E–W trending stretching lineation (Figs. 3b, 5b: 1–2). On the contrary, towards the structurally higher levels of Limb 1, the isoclinally folded metabasite layering S1 shows F2 folds with subhorizontal but N–S trending axes (Fig. 5b: 1). The F2 folds in Limbs 2 and 3 are non-cylindrical (Fig. 3a, c) with the fold axes orientation ranging from subhorizontal N–S trending to gently eastward plunging (Fig. 5b: 3–4). The non-cylindrical character of F2 folds is mostly associated with the superposition of N–S trending fold axes during the later N–S shortening related to D3 (Fig. 3a). However, Limb 2 also shows non-cylindrical isoclinal F2 folds with fold axes orientation changing from N–S to E–W (Fig. 3c), which lack the overprinting relations.

3.3. D3 deformation

The third deformation event D3 is associated with upright folding and local development of steep axial planar and low-grade cleavages resulting from generally N–S directed shortening. The trend of the fold axial planes AP3 and cleavages S3 gradually changes from WNW–ESE in the east to WSW–ENE in the west of the studied area (Fig. 5c: 1 to 5). Due to the gradual east to west decrease in dip angle of S2/S1 (Fig. 5a: 1 to 7), prior to D3 folding, the fold axes FA3 are steep in Limb 1 in the east and become shallow to subhorizontal in Limbs 2 and 3 towards the west (Fig. 5d: 1 to 5). In the N–S trending orthogneiss bodies, the orthogonal geometry of S2/S1 foliation and overprinting S3 cleavage locally resulted in their strongly constrictional appearance. The intersection of the two fabrics is parallel to both stretching lineation L2 and L1, and fold axes FA3 (cf. Fig. 5b and d). The F3 folds occur at all scales ranging from crenulation cleavages to kilometre-scale folds (Figs. 2, 3f–h and 4). A kilometre-scale F3 antiform has been identified in the western Limbs 2 and 3, where metabasites and metavolcanites occupy the core of the antiform (Figs. 2, 4 and 5a: 6). In the eastern Limbs 1 and 2, only smaller-scale F3 folds were identified, probably due to the presence of the thick tabular orthogneiss body. The asymmetry and folding patterns of F3 folds observed at the outcrop scale show parasitic folds consistent with the kilometer-scale F3 antiform in the western part of Limbs 2 and 3. In contrast, towards the east the asymmetry of the F3 folds is controlled by the geometry of the isoclinal mega-fold F2 so that the gently N–NE-dipping Limb 2 in its eastern part shows top-to-the-south F3 vergence (Fig. 3f) and the gently S–SE-dipping Limb 1 shows top-to-the-north F3 vergence.

In the vicinity of the Krkonoše-Jizera pluton, the S2 and S3 structures are overprinted by the contact and structural aureole related to the emplacement of this composite body (Žák et al., 2013).

3.4. D4 deformation

The deformation event D4 affecting the entire studied area is associated with the local development of centimetre- to decimetre-scale folds and kink bands with steep to moderately-dipping and generally NNE–SSW trending axial planes S4 and subhorizontal to moderately plunging axes. These F4 folds clearly overprint the F3 folds in Limb 2 (Fig. 3h). On the other hand, we cannot exclude a possibility that similar kink bands in Limb 1 with their axes perpendicular to lineation L2 may represent pre-D3 structures related to the last increments of the D2 deformation. This ambiguity stems from the lack of interference between D3 and D4 structures in Limb 1.

4. Quartz deformation microstructures

Analyses of quartz deformation microstructure and texture were carried out in samples of orthogneiss and deformed quartz veins collected from the main U-shaped orthogneiss body covering Limbs 1 and 2, as well as from the hinge 1 zone of the mega-scale isocline (for location see Figs. 1b, 2b). These analyses were aimed at the characterisation of the individual deformation fabrics and internal structure of the orthogneiss body with the main focus given to the conditions and kinematics of the studied deformation events. The orthogneiss shows evidence for three deformation fabrics S1, S2 and S3; however, the S1 and S2 show identical quartz deformation microstructures and only S3 is microstructurally distinct. In the orthogneiss, the quartz aggregates are recrystallised, strongly elongated and define S1 and S2 foliation, and L1 and L2 lineation. The original magmatic porphyroclasts of K-feldspar and plagioclase show syndeformational chemically-driven decomposition. The S1 and S2-related quartz microstructure is characterised by relatively large recrystallised grains with lobate boundaries (Fig. 6a–c) typical for the transition between subgrain rotation and grain boundary migration recrystallisation regimes (Stipp et al., 2002a; Jeřábek et al., 2007). The shape preferred orientation of quartz grains, the grain fabric, is frequently oblique to the S1 and S2 foliations. The S3-related quartz microstructure overprints the S1 and S2 microstructure and the degree of overprint can vary from serration of the larger S1 and S2-related quartz grains (Fig. 6b) to intense recrystallisation (Fig. 6d). The S3-related quartz microstructure is characterised by small recrystallised grains occupying the triple junctions of larger S1 andS2-related grains (Fig. 6d). Such a feature is typical for a low temperature bulging recrystallisation regime (Stipp et al., 2002a; Jeřábek et al., 2007). Assuming the typical natural strain rates of 10^{-14}–10^{-12} s^{-1} and water saturated conditions, the observed microstructures associated with the S1 and S2 fabrics suggests higher temperature conditions of ~450–500 °C whereas microstructure of the S3 cleavage suggests lower temperature conditions of ~300 °C(cf. Stipp et al., 2002a, b; Jeřábek et al., 2007).

5. Quartz textures

The crystal preferred orientation (CPO) of recrystallised quartz grains related to the S1 and S2 microstructure has been determined by the electron back-scattered diffraction method from XZ sections of the finite strain ellipsoid. To collect the CPO data, we used a hkl-device attached to a scanning electron microscope TESCAN Vega at the Institute of Petrology and Structural Geology in Prague with measuring conditions set to 20 kV acceleration voltage, 39 mm working distance, ~5 nA beam current and 70° sample tilt.

The CPO of recrystallised quartz was determined at 22 localities from quartz veins and orthogneiss samples marked as Q and G in Figure 7, respectively. In order to compare the asymmetric CPO patterns among individual samples, the resulting pole diagrams are presented in the same geographic reference frame defined by common, generally E–W, orientation of the stretching lineation (Fig. 7). The most typical CPOs in the analysed samples show single maxima or single and crossed girdles of c-axes implying activation of basal <a>, rhomb <a+c> and prism <a> slip systems (e.g. Schmid and Casey, 1986) in a dislocation creep regime . The inclination of single girdles with respect to the S1 and S2 foliations in the <c>-axis and <a>-axis pole figures (Lister and Williams, 1979; Simpson and Schmid, 1983; Schmid and Casey, 1986) indicates a prevailing top-to-the ESE shear sense associated with S2 overprinting S1 fabric in the isoclinal mega-folds of Limbs 1 and 2 and a prevailing top-to-the WNW shear sense associated with the S1 fabric in the hinge of this large-scale isocline (Fig. 7). The observed shear senses inferred from inclination of <c>-axis and <a>-axis CPOs are consistent with the shear senses suggested by the obliquity between the quartz grain shape preferred orientation and the S1 and S2 foliation trends (Fig. 6b, c; see e.g. Berthé et al., 1979; Simpson and Schmid, 1983).

6. Metamorphic record in phyllite and orhogneiss

The petrological study presented in this work wasconcentrated on the garnet-free phyllites from the east and west of the studied Krkonoše-Jizera Massif (Fig. 1b) and also on evaluation of the metamorphic record in different orthogneiss fabrics. Chemical analyses of particular minerals were performed by using a Cameca SX100 microprobe at the Masaryk University in Brno with operating conditions of 15 kV accelerating voltage and 10 nA beam current. The representative chemical analyses of minerals are listed in Table 1. The abbreviations of minerals in the text and figures follow Kretz (1983) with the exception of garnet (Gt).

6.1. Orthogneiss

The orhogneiss consists of relict magmatic porphyroclasts of K-feldspar and plagioclase that are overprinted by the metamorphic assemblage Ab-Ms-Kfs-Qtz (Fig. 8a, b) and accessory apatite, monazite and opaque minerals. Three orthogneiss samples were selected for chemical analysis of white mica composition in relation to the observed deformation fabrics. These samples come from the S2/S1 fabrics in Limbs 1 and 2 (VU88, EL 211; for localisation see Fig. 7) and from the S1 fabric in hinge 1 (EL159) of the F2 mega-fold. As mentioned earlier, the S1 and S2 fabrics are similar in macroscopic appearance. Our microscopic analysis also indicates that the two fabrics consist of identical mineral assemblages and quartz deformation microstructures (cf. 6a–c). However, a difference between the two fabrics was revealed by chemical analyses of white mica (Fig. 8a, b and Table 1). Thus while the S1 fabric from sample EL159 bears only highly phengitic white mica with Si ranging between 3.4 and 3.5 atoms per formula unit (a.p.f.u.), the white mica in samples VU88 and EL211 from the S2/S1 fabric shows higher scatter of Si content ranging between 3.2 and 3.46 a.p.f.u. (Table 1). The latter samples clearly show two generations of white mica (Fig. 8b and Table 1) with highly phengitic (Si=3.4–3.46 a.p.f.u.) cores of larger grains and less phengitic (Si=3.2–3.3 a.p.f.u.) rims and matrix grains. This pattern corresponds to an overprint of S1 by the parallel S2 fabric.

6.2. Phyllite

Two phyllite samples, EL9/2 and EL217, from the west (Limb 3) and east (Limb 1), respectively, were selected for detailed analysis (for location see Fig. 1b). Both samples are characterised by the garnet-free, but chloritoid-bearing assemblage Cld-Chl-Ms-Qtz±Pg with accessory apatite, tourmaline and monazite in the matrix (Fig. 8c, d). Chloritoid forms small elongated grains, which are in some cases transversal to the observed metamorphic foliation (Fig. 8c). On the other hand, where the foliation is dominated by white mica with a high degree of preferred orientation (probably S2), chloritoid grains are also parallel to this dominant foliation (Fig. 8d). Chloritoid is rich in manganese and has X_{Mg} (X_{Mg}=Mg/(Fe+Mg)) of 0.08–0.09 in sample EL9/2 and 0.12–0.16 in sample EL217 (Table 1). Chlorite is abundant in both samples and its X_{Mg} ranges between 0.35 and 0.36 in sample EL9/2 and between 0.46 and 0.52 in sample EL217 (Table 1). The white mica is phengitic muscovite, represented by the Ms-Cel-Pg-Bt solid solution with 4–13 mol% of paragonite, 11–30 mol% of celadonite and 0–3 mol% of biotite in both samples. Si content of phengitic muscovite ranges between 3.17 and 3.21 a.p.f.u. in sample EL9/2 and between 3.11 and 3.29 a.p.f.u. in sample EL217 (Table 1).

In order to characterise metamorphic P-T conditions of phyllite, the observed mineral assemblage and mineral chemistry were interpreted on the basis of phase equilibrium modelling and the P-T section approach. The bulk rock compositions used in the calculations correspond to the whole rock compositions obtained by the X-ray fluorescence (XRF) analysis. The P-T sections (Fig. 9) were calculated using the thermodynamic software package Perple_X (Connolly, 2005: version 6.6.6) with the internally consistent thermodynamic dataset of Holland and Powell (1998: 2004 upgrade). Mixing properties of phases used in the calculations were taken from Berman (1990) for garnet, Newton et al. (1980) for plagioclase, Coggon and Holland (2002) for white mica, Holland et al. (1998) for chlorite and Powell and Holland (1999) for biotite, staurolite and chloritoid. The manganese end-members for the biotite, staurolite and chloritoid solid solution mixing models in question were incorporated after Tinkham et al. (2001). Regarding the observed mineral assemblage and chemical composition of studied minerals, the P-T sections for both samples were calculated in the system MnO-Na_2O-CaO-K_2O-FeO-MgO-Al_2O_3-SiO_2-H_2O (MnNCKFMASH) with H_2O in excess.

The P-T section for sample EL9/2 was calculated with the following molar bulk-rock composition: MnO = 0.10, Na_2O = 1.31, CaO = 0.03, K_2O = 3.06, FeO = 6.45, MgO = 3.16, Al_2O_3 = 15.86 and SiO_2 = 70.03. In the resulting P-T section (Fig. 9a), the temperature-dependent stability of the observed mineral assemblage Cld-Chl-Ms-Qtz-Pg is restricted by the garnet-in reaction at higher temperatures and lawsonite-out reaction at lower temperatures. A more precise estimate of pressure conditions can be calculated based on the celadonite component in muscovite. Thus, by using compositional isopleths of X_{Mg} in chloritoid and Si in muscovite (Table 1), the equilibrium P-T conditions of the mineral assemblage in sample EL9/2 correspond to 400–450 °C at 14–16 kbar (Fig. 9a).

The P-T section for sample EL217 was calculated with the following molar bulk-rock composition: MnO = 0.18, Na_2O = 0.89, CaO = 0.08, K_2O = 2.78, FeO = 7.51, MgO = 3.99, Al_2O_3 = 16.06 and SiO_2 = 68.51. In the resulting P-T section (Fig. 9b), the temperature-dependent stability of the observed mineral assemblage Cld-Chl-Ms-Qtz-Pg is again restricted by the lawsonite-out and garnet-in reactions. Compared to the calculation result for sample EL9/2 (Fig. 9a), the lawsonite-out reaction curve is shifted to slightly higher temperatures. The temperature-dependent compositional isopleths of X_{Mg} in chloritoid in sample EL217 (Table 1) again constrain the temperature range of the observed mineral assemblage while the pressure dependent celadonite component in muscovite (Table 1) constrains the pressure range. Thus the Si content in muscovite together with the X_{Mg} in chloritoid and X_{Mg} in chlorite (Table 1) suggests high-pressure metamorphic P-T conditions of 14–18 kbar at 450–520°C (Fig. 9b).

7. Discussion

7.1. Metamorphic and lithostratigraphic structure of the Krkonoše-Jizera Massif

It has been generally accepted that the Krkonoše-Jizera Massif represents a subduction-accretionary complex associated with the southeastward subduction of the Saxothuringian oceanic and continental crust below the Teplá-Barrandian domain (Matte et al., 1990; Pin et al., 1998; Franke and Żelaźniewicz, 2000; Mazur and Aleksandrowski, 2001). The complex is occupied by the lower plate rocks, which experienced HP-LT metamorphism (Cháb and Vrána, 1979; Guiraud and Burg, 1984; Patočka et al., 1996; Žáčková et al., 2010; Faryad and Kachlík, 2013). In the current erosion section, this E–SE dipping wedge-shaped complex shows steep hanging wall and flat footwall contacts (Fig. 4) and its spatial extent is limited by the lower-pressure metabasite Leszczyniec Unit in the east and the par-autochthonous Ještěd Unit in the west. In the original nappe concept (Mazur, 1995; Mazur and Kryza 1996; Seston et al., 2000; Mazur and Aleksandrowski, 2001), the HP core of the Krkonoše-Jizera Massif has been associated with two nappes, the lower and the middle thrust sheet, distinguished on the basis of lithology, geochronological data and inverted metamorphic field gradient (Kryza and Mazur, 1995). The metamorphic inversion has recently been contradicted by the P-T estimates of 460–520 °C at 18–19 kbar (M1 of Žáčková et al., 2010; Faryad and Kachlík, 2013, see Fig. 10) as these conditions indicate much higher pressures in the lower thrust sheet compared to the earlier estimates of 300–530°C at 6.5–12 kbar from blueschists in the middle thrust sheet (Kryza and Mazur, 1995; Smulikowski, 1995; Patočka et al., 1996). However, our new P-T estimates of 400–520°C at 14–19 kbar (Figs. 9, 10), calculated for chloritoid-bearing phyllite from the structurally lower part of the middle thrust sheet, document comparable P-T conditions in both thrust sheets (Fig. 10). In addition, the phengitic white mica in the orthogneiss from the lower thrust sheet, documented in this study (Fig. 8a, b and Table 1), indicates high-pressure conditions. These new results suggest that the HP metamorphism probably affected the entire wedge complex of the Krkonoše-Jizera Massif.

The distinction of the two nappes, however, can still be made based on the available geochronology with several older Ar-Ar phengite and muscovite ages from blueschits in the middle thrust sheet (364–345 Ma with a typical error of ±2 Ma, Maluski and Patočka, 1997; Marheine et al., 2002) contrasting with the younger U-Pb monazite ages and numerous Ar-Ar muscovite ages from the lower thrust sheet (340–330 Ma with a typical error of ±3 Ma for Ar-Ar and ±6 Ma for U-Pb, Marheine et al., 2002; Žáčková et al., 2010). In addition, lithological differences between the two thrust sheets, characterised by metapelites interlayered with metabasites prevailing in the middle thrust sheet and metapelites with quartzites that dominate the lower thrust sheet, likely correspond to a progressive subduction of more distal and proximal sedimentary sequences of the Saxothuringian passive margin (Winchester et al., 2003), respectively.

The nappe structure of the HP wedge complex is relatively simple in the eastern part of the Krkonoše-Jizera Massif, where the middle and lower thrust sheets are formed by several lithological belts consisting, from top to bottom (for numbering see Figs. 1b and 2b), of mafic blueschists (4) – a possible relic of the Saxothuringian oceanic crust; garnet-free micaschist, phyllite and metavolcanics

(3) – a distal volcano-sedimentary succession of the Saxothuringian passive margin; orthogneiss (2) – a slice of the Saxothuringian basement; garnet-bearing micaschist (1) – a proximal sedimentary succession of the Saxothuringian passive margin. On the contrary, towards the west this simple nappe structure starts to be complicated as the middle thrust sheet occurs in the footwall position of the lower thrust sheet. Although such an inverted structure may be explained by its duplication related to, e.g., out of sequence thrusting, the geometry of deformation fabrics and of individual lithological belts (1–4) suggests that the observed pattern corresponds to the geometry of large-scale isoclinal folds reconstructed in Figure 2. Moreover, the lack of major metamorphic gaps manifested by comparable P-T conditions obtained along the entire length of the single lithological belt (3) winding across the entire HP wedge complex (cf. samples EL9/2 and EL217 in Figs. 1b, 2 and 10) support the fold interpretation. The slightly lower temperature and perhaps also pressure conditions estimated for the western part of the middle thrust sheet (sample EL9/2) compared to its eastern part (sample EL217) can be explained by a different depth of burial prior to folding.

7.2. Nappe stacking during cold underplating of high-pressure thrust sheets

The nappe structure of the Krkonoše-Jizera HP wedge seems to record a continuous process of subduction and underplating of imbricated slices derived from the Saxothuringian lower plate to the base of the upper plate (Fig. 11a) interpreted as a northern continuation of the Teplá-Barrandian Unit (Mazur and Alexandrowski, 2001; the Teplá-Barrandian domain of Schulmann et al., 2014). With this respect the upper thrust sheet, represented by the lower-pressure Leszczyniec metaigneous complex (Kryza et al., 1995), has been previously interpreted as an accreted fragment of the Saxothruringian oceanic crust (Mazur and Alexandrowski, 2001). A similar nappe structure of an accreted oceanic crust and underlying subducted/underplated passive margin has been recently reported from the Tavşanlı zone in west Turkey (Plunder et al., 2015). Alternatively, the Leszczyniec complex may represent the lower crust of the upper plate as it comprises numerous felsic rocks and metagabbro with aU-Pb zircon age of 494±2 Ma (Oliver et al., 1993). This age corresponds to a period of extensive Cambro-Ordovician continental rifting related to the subsequent opening of the Saxothuringian/Rheic Ocean. Similar metagabbroic complexes of identical age occur further to the SW where they intrude the base of the Teplá-Barrandian Unit s.s. (Štědrá et al., 2002; Timmermann et al., 2004; Jašarová et al., subm.; Peřestý et al., subm.).

In this context, the first clearly identified allochthonous slice that was attached to the upper plate is represented by the metabasites (belt (4) in Figs. 2b and 1b) of the middle thrust sheet that contain relics of blueschist facies metamorphism (Fig. 11a). It is not clear if the mafic blueschists represented an oceanic crust or they belonged to the volcano-sedimentary sequence of the distal part of the Saxothuringian passive margin. However, the spatially associated distal margin metasediments and metabasites (belts (3) and (4) in Figs. 2b and 1b) have been merged into the middle thrust sheet until additional data on this issue are available. The second allochthonous slice, subsequently attached to the upper plate, is represented by the lower thrust sheet formed by an imbricated slice of basement orthogneiss and metasedimentary cover of the proximal part of the Saxothuringian passive margin. It is not clear whether the orthogneiss and metasediments (belts (2) and (1) in Figs. 2b and 1b) represent a thick basement-cover slice that became overturned in the subduction channel and attached to the upper plate, or if they are two separate thin slices that were successively attached to the upper plate.

It is interesting to explore the possibly thick-skinned (cover + basement) character of the lower thrust sheet in contrast to the thin-skinned (only cover) character of the middle thrust sheet. Recent numerical simulations demonstrated the importance of viscosity contrast at the basement-cover interface for the formation of thin-skinned nappes, with high basement-cover viscosity contrast, versus thick-skinned nappes, with low viscosity contrast (Bauville and Schmalholz, 2015). Passive margins are typically associated with the fine-grained sediments in distal sequences (phyllite) and the coarse-grained sediments in proximal sequences (quartzite) imposing high and low basement-cover viscosity contrasts, respectively. Therefore the conclusions of Bauville and Schmalholz (2015) provide a good reasoning for transition from the thin- to thick-skinned nappes developed as a consequence of progressive subduction of distal and proximal parts of the passive margin (cf. Burov et al., 2014).

The juxtaposition of individual nappes in the Krkonoše-Jizera Massif has been previously associated with northwestward thrusting during D1 deformation (Mazur and Kryza, 1996; Mazur and Alexandrowski, 2001). Similar, top-to-the WNW, shear sense for the D1 deformation was also concluded in this study from the crystallographic preferred orientation of recrystallised quartz veins deformed parallel to the S1 fabric in the orthogneiss (Figs. 6 and 7). These shear senses occur exclusively in the hinge zones of large-scale isoclinal folds F2 where the S1 fabric, associated with phengitic white mica (Fig. 8a), was later passively rotated into a steep E–W trending orientation. The analysed quartz microstructure in S1 indicates its development at 450–500 °C (cf. figure 6b and microstructural calibrations of Stipp et al. 2002b; Jeřábek et al., 2007) that coincides with the temperature estimates for both M1 and M2 events of Žáčková et al. (2010) shown in Figure 10. For this reason it is not clear if the nappe stacking occurred during the M1 or M2 event. However, the relict form of the peak-pressure assemblage M1 represented by chloritoid inclusions in garnet cores (Žáčková et al., 2010), contrasting with the dominance of the matrix assemblage M2 of Žáčková et al. (2010) in the S1 fabric in metapelites, suggests that thrusting occurred at M2 conditions. An alternative scenario where the S1 fabric formed during continuous exhumation from M1 (18–19 kbar) to M2 (10.5–13.5 kbar) pressure conditions is inconsistent with the observed thrust kinematics associated with S1, because synkinematic exhumation would lead to a normal-sense movement. The observed kinematics thus suggests that the HP nappes were exhumed to the M2 pressures prior to the formation of S1 and the associated overprint of an earlier fabric by M2 metamorphic conditions. S1-M2 is thus interpreted as reflecting the deformation associated with underplating/attachment of individual nappes to the base of the thickened upper plate (Fig. 11a) during ongoing underthrusting of the lower plate, which is the only mechanism that can explain the formation of the observed thrust kinematics. With the absence of earlier (pre-S1) deformation fabrics, it is difficult to identify unequivocally the mechanism responsible for M1 to M2 exhumation. However, it is very likely that the adiabatic character of the M1 to M2 partial exhumation (Fig. 10) reflects exhumation in the subduction channel. Here, the difference in density between subducted continental material and surrounding mantle is high and therefore buoyancy-driven exhumation appears likely (e.g. Chemenda et al., 1995; Hacker and Gerya, 2013; Burov et al., 2014).

7.3. Large-scale folding and exhumation of the nappe stack

Formation of the isoclinal mega-folds F2 covering the entire region of the Krkonoše-Jizera HP wedge complex (Fig. 2) is accompanied by the development of an axial planar cleavage S2 and associated greenschist facies overprint of the S1 fabric. This folding thus documents the exhumation/transition from the M2 to M3 metamorphic assemblage with estimated P-T conditions of 470–520 °C at 10.5–13.5 kbar and <480 °C at <8.5 kbar, respectively (Žáčková et al., 2010 in Fig. 10). The transition between the two assemblages/fabrics is rather continuous as manifested by the stability of MP phases (garnet or chloritoid) in the S2 cleavage of some samples (Figs. 3d and 8c, d). At the same time, S2 is also associated with the widespread blastesis of albite (Fig. 3d, e, g) occurring at 350–450 °C and 3–7 kbar (M3 of Žáčková et al., 2010 in Fig. 10) and showing syn- to mostly post-kinematic relationship with respect to S2 (cf. Fig. 3d, g). The blastesis affecting nearly the entire studied region may reflect the decompression-related breakdown of paragonite (Konopásek, 1998) suggesting that the higher pressure conditions are indeed characteristic for most rocks of the Krkonoše-Jizera Massif. At the same time, the syn-exhumation deformation of orthogneiss could have led to metasomatic enrichment of metapelites by sodium (Žáčková et al., 2010), though the unequivocal spatial association of albite blastesis and the presence of orthogneiss has not been demonstrated.

The metamorphic and deformation record in the Krkonoše-Jizera Massif suggests that the HP-MP nappes were exhumed from similar depths, marked by M2 metamorphic conditions, via combination of large-scale folding and formation of detachment and thrust zones along the contact with the upper and lower plates (Fig 11b), respectively (e.g. Xypolias and Koukouvelas, 2001; Searle et al., 2004; Agard et al., 2010). In this respect, it is worth to note the change in the sense of shear revealed by the quartz deformation microstructures and textures along the folded orthogneiss body (Figs. 2, 6 and 7). Figure 7 demonstrates that the hinge zones of the F2 mega-folds, dominated by the passively rotated S1 fabric, are associated with the top-to-the WNW tectonic transport while the limbs, characterised by S2 overprinting S1 relations, show the opposite top-to-the ESE shear sense. In the overturned Limb 2, this change may be explained by both its passive 180° rotation, leading to reorientation of the incipient shear sense related to D1 nappe stacking (e.g. Stünitz et al., 1991; Morales et al., 2011), or D2 overprint. In Limb 1; however, this change is clearly related to S2 overprint and formation of a detachment zone allowing for exhumation of the HP nappe stack. This interpretation is in a good agreement with extensional detachment structures that have been reported from the uppermost part of Limb 1 namely along the contact with the hanging wall Leszczyniec Unit where the Leszczyniec detachment shear zone was identified (Mazur and Kryza, 1996; Seston et al., 2000; Mazur and Aleksandrowski, 2001). The internal part of the folded nappe stack, specifically the central part of Limb 2, shows additional evidence for top-to-the WNW thrusting manifested by the development of highly noncylindrical isoclinal folds F2 (Fig. 3c) and associated reorientation of originally N–S trending fold axes towards the generally E–W orientation parallel to the stretching lineation (cf. Figs. 2 and 5). The central part of Limb 2, however, does not show any evidence for a major discontinuity in neither metamorphic nor structural pattern and therefore it is very likely that it documents differential movements related to the development of the F2 mega-folds and synchronous overall top-to-WNW exhumational transport. On the contrary, the basal contact of the HP wedge with the relatively low-grade metamorphic rocks of the par-autochthonous unit in the east is associated with a major gap in metamorphic conditions and therefore must represent a major thrust discontinuity in the Krkonoše-Jizera Massif (Kachlík and Kozdrój, 2001).

The orientation pattern of small-scale folds F2 characterised by nucleation at high angles to the transport direction contrasts with the transport-parallel orientation of hinges of the F2 mega-folds (cf. Figs. 2 and 5). It is not clear if such a geometry may reflect a complicated sheath fold structure (e.g. Alsop and Holdsworth, 2012) or flow-perturbation folding related to lateral velocity gradients in the exhumation channel (see Alsop and Holdsworth, 2007; Xypolias and Alsop, 2014). The latter alternative may be a more realistic explanation of the observed geometry as the transport-perpendicular nucleation and subsequent rotation of mega-folds would demand high strain transfer zones inside the folded stack that are not evident from our structural observations.

The high-pressure metamorphic nappe stack of the Krkonoše-Jizera Massif was exhumed from a wedge-shaped domain between the easterly Teplá-Barrandian upper plate and the westerly Saxothuringian lower plate. The small scale structures together with the development of F2 mega-folds and overall flattening of exhumation fabric S2 away from the upper plate contact (Figs. 4 and 5) suggests a geometry of an antiformal stack structure that is typical for accretionary orogenic wedges (Malavieille, 2010). It is expected that the increasing thickness of the subducted passive margin leads to a switch from continental subduction to continental collision at late stages of the convergence (e.g. Burov et al., 2014). The consequent shortening in the wedge domain together with an increase in basal friction and mechanical coupling along the subduction interface can explain the development of the large-scale forced folds F2 and associated exhumation of the HP nappe stack (Fig. 11b). The M2 to M3 exhumation of the HP wedge may thus be accommodated by the shortening of the accretionary wedge induced by the two colliding crustal blocks at late collisional stages (Platt, 1986; Platt, 1993; Burov et al., 2014).

The last increments of exhumation in the Krkonoše-Jizera Massif are associated with the D3 folding induced by N–S horizontal shortening (Figs. 3 and 5) that is recorded elsewhere in the Bohemian Massif (e.g. Konopásek et al., 2001; Edel et al., 2003). The D3 folding occurred prior to intrusion of the Krkonoše-Jizera composite pluton (~320–315 Ma), manifested by the contact aureole overprinting the F3 folds, and implying Early Carboniferous age of this deformation (Marheine et al., 2002; Žák et al., 2013). Open and asymmetric character of F3 folds reported from the northern part of the West Sudetes (Seston et al., 2000), contrasting with the local development of tight and cleavage bearing F3 folds in the southern part of the Krkonoše-Jizera Massif, may be attributed to the decreasing intensity of D3 towards the north.

7.4. The Krkonoše-Jizera Massif in the context of the Variscan evolution of the Bohemian Massif

The subduction of the Saxothuringian passive margin has been recently associated with the major return of the buoyant lower-plate-derived felsic crust from the subduction channel to the base of the upper plate Teplá-Barrandian domain (Lexa et al., 2011; Schulmann et al., 2009; 2014) following the relamination concept of Hacker et al. (2011). The material from the relaminated/thickened forearc domain had been subsequently redistributed by lower crustal flow towards the easterly core of the Bohemian Massif represented by the Moldanubian domain (Chopin et al., 2012; Schulmann et al., 2014; Maierová et al., 2014; Dymková et al., 2016). This interpretation is now supported by an increasing amount of evidence for a two-stage P-T evolution of orogenic granulites in the Moldanubian domain showing an early HP-(MT–HT) stage followed by MP-HT stage (Nahodilová et al., 2014; Jedlička et al., 2015). In this context, the M1 to M2 buoyancy-driven partial exhumation of the Krkonoše-Jizera HP rocks from deeper parts of the subduction channel to the base of the upper plate may coincide with major underplating/thickening of the forearc Teplá-Barrandian domain. With this respect the contrasting temperature record of medium-pressure metamorphism in the Moldanubian granulites (<840°C; Nahodilová et al., 2014) and in the Krkonoše-Jizera metasediments (<520°C; Žáčková et al., 2010) can be explained by the cold thermal regime in the vicinity of the ongoing subduction/underthrusting of the Saxothuringian plate and elevated heat flow due to radiogenic heat production in the easterly orogenic root domain (Lexa et al., 2011).

Recent tectonic models for the Bohemian Massif further suggest that the post-relamination exhumation of the originally high-pressure units in both the easterly orogen core and the westerly suture zone is associated with compression-driven exhumation at the late collisional stage (Chopin et al., 2012; Jastrzębski et al., 2014; Maierová et al., 2014). During this stage the lower crustal rocks in the orogen core of the Moldanubian domain were exhumed within the cores of large-scale antiformal structures (Štípská et al., 2004; Schulmann et al., 2005, 2014). In contrast, the late exhumation history of high pressure rocks in the former subduction channel is still poorly understood (Nasdala and Massonne, 2000; Konopásek and Schulmann, 2005; Kotková et al., 2011). In this context it is interesting to note the two-stage exhumation history of the subduction complex in the Krkonoše-Jizera Massif described in this work.

8. Conclusions

The Krkonoše-Jizera Massif provides a new input to understanding of the Variscan subduction-exhumation process in the Bohemian Massif. The lithostratigraphic and metamorphic data from the studied region document a wide extent of the subduction-related HP-LT metamorphism M1 recorded within the two main nappes derived from distal and proximal parts of the subducted Saxothuringian passive margin. The new P-T estimates calculated for two chloritoid-bearing phyllite samples in the lower part of the upper nappe (middle thrust sheet) revealed 400–450 °C at 14–16 kbar and 450–520 °C at 14–18 kbar for the westernmost and easternmost parts of the studied area, respectively. These estimates are in a good agreement with the previous data and suggest nearly 50 km lateral extent of the HP metamorphic rocks. At the same time, the repetitive pattern of four lithologically distinct belts winding across the studied area can be interpreted in accordance with the structural data and suggest the presence of mega-scale isoclinal folds. Quartz deformation microstructures and textures in quartz veins deformed parallel to the main deformation fabrics provided systematic information on deformation kinematics showing thrusting in the hinge zone and normal sense of shearing in the limbs of the mega-folds. It is concluded that the thrusting occurred during deformation D1, that was associated with the still HP-LT metamorphic assemblage M2 formed at 470–520 °C and 10.5–13.5

kbar. D1-M2 reflects stacking of the two nappes and their successive attachment to the base of the Teplá-Barrandian upper plate. The later normal sense of shearing is associated with folding and deformation D2 characterised by a continual decrease in metamorphic conditions to the greenschist facies (M3) at 350–450 °C and 3–7 kbar, and reflects exhumation of the nappe stack. The proposed two-stage exhumation of HP-LT rocks from the subduction channel is based on recognition of three distinct metamorphic assemblages (M1–M3) associated with two kinematically distinct deformation fabrics (D1 and D2). The first stage of exhumation is marked by the change from HP-LT conditions of M1 to the still HP-LT conditions of M2. With its adiabatic character, this partial exhumation is interpreted as a buoyancy-driven return of material from the subduction channel leading to underplating of the Teplá-Barrandian upper plate reflected by the D1-M2. The second stage of exhumation is marked by a continual decrease in both P and T conditions from HP-LT, associated with M2-D1, to LP-LT conditions, associated with M3-D2. This later exhumation is marked by the development of isoclinal mega-folds F2 and interpreted as a result of shortening in the accretionary wedge indicating a switch from continental subduction to continental collision at the late stages of convergence.

Acknowledgement

This work was supported by the field mapping project of the Czech Geological Survey no. 390001 and by the Czech Science Foundation (GACR) research grant no. 13-16315S. K. Schulmann and O. Lexa are thanked for numerous valuable discussions during the progress of this work. S. Mazur and M. Stipp are thanked for numerous suggestions for improvements in their reviews and J. Hippertt is thanked for careful editorial work.

References

Agard, P., Searle, M.P., Alsop, G.I., Dubacq, B., 2010. Crustal stacking and expulsion tectonics during continental subduction: P-T deformation constraints from Oman. Tectonics 29, 1–19.

Agard, P., Vitale-Brovarone, A., 2013. Thermal regime of continental subduction: The record from exhumed HP-LT terranes (New Caledonia, Oman, Corsica). Tectonophysics 601, 206–215.

Alsop, G.I., Holdsworth, R.E., 2012. The three dimensional shape and localisation of deformation within multilayer sheath folds. J. Struct. Geol. 44, 110–128.

Alsop, G.I., Holdsworth, R.E., 2007. Flow perturbation folding in shear zones, in: Ries, A.C., Butler, R.W.H., Graham, R.D. (Eds.), Deformation of the Continental Crust: The Legacy of Mike Coward. Geol. Soc. London Spec. Pub. 272, 75–101.

Bauville, A., Schmalholz, S.M., 2015. Transition from thin- to thick-skinned tectonics and consequences for nappe formation: Numerical simulations and applications to the Helvetic nappe system, Switzerland. Tectonophysics 665, 101–117.

Berman, R.G., 1990. Mixing properties of Ca-Mg-Fe-Mn garnets. Am. Mineral. 75, 328–344.

Berthé, D., Choukroune, P., Jégouzo, P., 1979. Orthogneiss, mylonite and non coaxial deformation of granites: the example of the South Armorican Shear Zone. J. Struct. Geol. 1, 31–42.

Borkowska, M., Hameurt, J., Vidal, O., 1980. Origin and age of Izera gneisses and Rumburk granites in the West Sudetes. Acta Geol. Pol. 30, 121–145.

Burov, E., Francois, T., Agard, P., Le Pourhiet, L., Meyer, B., Tirel, C., Lebedev, S., Yamato, P., Brun, J.P., 2014. Rheological and geodynamic controls on the mechanisms of subduction and HP/UHP exhumation of crustal rocks during continental collision: Insights from numerical models. Tectonophysics 631, 212–250.

Cháb, J., Vrána, S., 1979. Crossite-actinolite amphiboles of the Krkonoše-Jizera crystalline complex and their geological significance. Věštník Ústř. úst. geol. 54, 143–150.

Chaloupský, J., 1989. Geology of the Krkonoše and Jizerské Hory Mountains. Ústř. úst. geol., Praha (in Czech with English summary).

Chemenda, A.I., Mattauer, M., Malavieille, J., Bokun, A.N., 1995. A mechanism for syn-collisional rock exhumation and associated normal faulting: Results from physical modelling. Earth Planet. Sci. Lett. 132, 225–232.

Chlupáč, I., 1993. Stratigraphic evaluation of some metamorphic units in the N part of the Bohemian Massif. Neues Jahrb. Geol. Palä. - Abhandl. 188, 363–388.

Chopin, F., Schulmann, K., Skrzypek, E., Lehmann, J., Dujardin, J.R., Martelat, J.E., Lexa, O., Corsini, M., Edel, J.B., Štípská, P., Pitra, P., 2012. Crustal influx, indentation, ductile thinning and gravity redistribution in a continental wedge: Building a Moldanubian mantled gneiss dome with underthrust Saxothuringian material (European Variscan belt). Tectonics 31, 1–27.

Cloos M. 1982. Flow melanges: Numerical modelling and geologic constraints on their origin in the Fransiscan subduction complex, California. Geol. Soc. Am. Bull. 93, 330–345.

Coggon, R., Holland, T.J.B., 2002. Mixing properties of phengitic micas and revised garnet-phengite thermobarometers. J. Metam. Geol. 20, 683–696.

Connolly, J.A.D., 2005. Computation of phase equilibria by linear programming: a tool for geodynamic modeling and it application to subduction zone decarbonation. Earth Planet. Sci. Letters 236, 524–541.

Dostál, J., Patočka, F., Pin, C., 2001. Middle/Late Cambrian intracontinental rifting in the central West Sudetes, NE Bohemian Massif (Czech Republic): Geochemistry and petrogenesis of the bimodal metavolcanic rocks. Geol. J. 36, 1–17.

Dymkova, D., Gerya, T., Burg, J.P., 2016. 2D thermomechanical modelling of continent-arc-continent collision. Gondwana Res. 32, 138–150.

Edel, J.B., Schulmann, K., Holub, F.V., 2003. Anticlockwise and clockwise rotations of the Eastern Variscides accommodated by dextral lithospheric wrenching: palaeomagnetic and structural evidence. J. Geol. Soc. London. 160, 209–218.

Faryad, S.W., Kachlík, V., 2013. New evidence of blueschist facies rocks and their geotectonic implication for Variscan suture(s) in the Bohemian Massif. J. Metam. Geol. 31, 63–82.

Franke, W., 2000. The mid-European segment of the Variscides: tectonostratigraphic units, terrane boundaries and plate tectonic evolution. In: Franke, E., Haak, V., Oncken, O., Tanner, D. (Eds.), Orogenic Processes: Quantification and Modelling in the Variscan Belt. Geol. Soc. London Spec. Pub. 179, 35–56.

Franke, W., Żelaźniewicz, A., 2000. The eastern termination of the Variscides: Terrane correlation and kinematic evolution. In: Franke, W., Haak, V., Oncken, O., Tanner, D. (Eds), Orogenic Processes: Quantification and Modelling in the Variscan Belt. Geol. Soc. London Spec. Pub. 179, 63–86.

Franke, W., Żelaźniewicz, A., Porębski, S. J., Wajsprych, B., 1993. Saxothuringian zone in Germany and in Poland: differences and common features. Geol. Rundsch. 82, 583–599.

Guiraud, M., Burg, J. P., 1984. Mineralogical and petrological study of a blueschist metatuff from the Zelezny Brod Crystalline Complex, Czechoslovakia. Neues Jahrb. Mineral. - Abhandl. 149, 1–12.

Hacker, B.R., Kelemen, P.B., Behn, M.D., 2011. Differentiation of the continental crust by relamination. Earth Planet. Sci. Lett. 307, 501–516.

Hacker, B.R., Abers, G.A., Peacock, S.M., 2003. Subduction factory 1. Theoretical mineralogy, densities, seismic wave speeds, and H2O contents. J. Geophys. Res. 108, 1–26.

Hacker, B.R., Gerya, T. V., 2013. Paradigms, new and old, for ultrahigh-pressure tectonism. Tectonophysics 603, 79–88.

Holland, T.J.B., Baker, R., Powell, R., 1998. Mixing properties and activity-composition relationships of chlorites in the system MgO-FeO-Al_2O_3-SiO_2-H_2O. Eur. J. Mineral. 10, 395–406.

Holland, T.J.B., Powell, R., 1998. An internally consistent thermodynamic data set for phases of petrological interest. J. Metam. Geol. 16, 309–343.

Hsu K J. 1971. Franciscan melange as a model for eugeosynclinal sedimentation and underthrusting tectonics. J. Geophys. Res. 76, 1162–1170.

Hyppolito, T., Juliani, C., Garcia-Casco, A., Meira, V., Bustamante, A., Hall, C., 2015. LP/HT metamorphism as a temporal marker of change of deformation style within the Late Palaeozoic accretionary wedge of central Chile. J. Metamorph. Geol. 33, 1003–1024.

Jašarová, P., Racek, M., Jeřábek, P., Holub, F.V. subm. Metamorphic reactions and textural changes in coronitic metagabbros from Teplá Crystalline and Mariánské-Lázně complexes, Bohemian Massif. J. Geosci.

Jastrzębski, M., Stawikowski, W., Budzyn, B., Orlowski, R., 2014. Migmatization and large-scale folding in the Orlica-Śnieżnik Dome, NE Bohemian Massif: Pressure-temperature-time-deformation constraints on Variscan terrane assembly. Tectonophysics 630, 54–74.

Jedlička, R., Faryad, S.W., Hauzenberger, C., 2014. Prograde metamorphic history of UHP granulites from the moldanubian zone (Bohemian Massif) revealed by major element and Y + REE zoning in garnets. J. Petrol. 56, 2069–2088.

Jeřábek, P., Faryad, W.S., Schulmann, K., Lexa, O., Tajčmanová, L., 2008. Alpine burial and heterogeneous exhumation of Variscan crust in the West Carpathians: insight from thermodynamic and argon diffusion modelling. J. Geol. Soc. London. 165, 479–498.

Jeřábek, P., Stünitz, H., Heilbronner, R., Lexa, O., Schulmann, K., 2007. Microstructural-deformation record of an orogen-parallel extension in the Vepor Unit, West Carpathians. J. Struct. Geol. 29, 1722–1743.

Jolivet, L., Faccenna, C., Goffé, B., Burov, E., Agard, P., 2003. Subduction tectonics and exhumation of high-pressure metamorphic rocks in the Mediterranean orogens. Am. J. Sci. 303, 353–409.

Kachlík, V., Kozdrój, W., 2001. Ještěd Range Unit. In: Kozdrój, W., Krentz, O. and Opletal, M. (Eds.), Comments on the Geological map Lauzitz - Jizera - Karkonozse (without Cenozoic sediments). Sächsisches Landesamt für Umwelt und Geologie/Bereich Boden und Geologie, Freiberg, Panstwowy Institut Geologiczny, Warzsawa. Český geolologický ústav Praha, Warzsawa, 27–31.

Kachlík, V., Patočka, F., 1998. Cambrian/Ordovician intracontinental rifting and Devonian closure of the rifting generated basins in the Bohemian Massif realms. Acta Univ. Carol. Geol. 42, 433–441.

Keppler, R., Stipp, M., Behrmann, J.H., Ullemeyer, K., Heidelbach, F., 2016. Deformation inside a paleosubduction channel - Insights from microstructures and crystallographic preferred orientations of eclogites and metasediments from the Tauern Window, Austria. J. Struct. Geol. 82, 60–79.

Konopásek, J., 1998. Formation and destabilization of the high pressure assemblage garnet-phengite-paragonite (Krušné Hory Mountains, Bohemian Massif): the significance of the Tschermak substitution in the metamorphism of pelitic rocks. Lithos 42, 269–284.

Konopásek, J., 2001. Eclogitic micaschists in the central part of the Krušné hory Mountains (Bohemian Massif). Eur. J. Mineral. 13, 87–100.

Konopásek, J., Schulmann, K., Lexa, O., 2001. Structural evolution of the central part of the Krušné hory (Erzgebirge) Mountains in the Czech Republic – evidence for changing stress regime during Variscan compression. J. Struct. Geol. 23, 1373–1392.

Konopásek, J., Schulmann, K., 2005. Contrasting Early Carboniferous field geotherms: evidence for accretion of a thickened orogenic root and subducted Saxothuringian crust (Central European Variscides). J. Geol. Soc. London 162, 463–470.

Korytowski, A., Dörr, W.,,, Żelaźniewicz, A., 1993. U-Pb dating of (meta)granitoids in the NW Sudetes (Poland) and their bearing on tectonostratigraphic correlation. Terra Nova 5, 331–332.

Kotková, J., O'Brian, P.J., Ziemann, M.A., 2011. Diamond and coesite discovered in Saxony-type granulite: Solution to the Variscan garnet peridotite enigma. Geology 39, 667–670.

Kretz, R., 1983. Symbols for rock forming minerals. Am. Mineral. 68, 277–279.

Kröner, A., Hegner, E., Hammer, J., Haase, G., Bielicki, K.H., Krauss, M., Eidam, J., 1994. Geochronology and Nd-Sr systematics of Lusatian granitoids: significance for the evolution of the

Variscan orogen in east-central Europe. Geol. Rundsch. 83, 357–376.

Kröner, A., Jaeckel, P., Hegner, E., Opletal, M., 2001. Single zircon ages and whole-rock Nd isotopic systematics of early Palaeozoic granitoid gneisses from the Czech and Polish Sudetes (Jizerské hory, Krkonoše and Orlice-Sněžník Complex). Int. J. Earth Sci. 90, 304–324.

Kryza, R., Mazur, S., 1995. Contrasting metamorphic paths in the SE part of the Karkonosze-Izera block (Western Sudetes, SW Poland). Neues Jahrb. Mineral. - Abhandl. 169, 157–192.

Kryza, R., Mazur, S., Pin, C., 1995. Leszczyniec meta-igneous complex in the eastern part of the Karkonosze-Izera Block, Western Sudetes: trace element and Nd isotope study. Neues Jahrb. Mineral. - Abhandl. 170, 59–74.

Kryza, R., Muszynski, A., Vielzeuf, D., 1990. Glaucophane-bearing assemblage overprinted by greenschist-facies metamorphism in the Variscan Kaczawa complex, Sudetes, Poland. J. Metam. Geol. 8, 344–355.

Kryza, R., Zalasiewicz, J., Mazur, S., Aleksandrowski, P., Sergeev, S., Larionov, A., 2007. Precambrian crustal contribution to the Variscan accretionary prism of the Kaczawa Mountains (Sudetes, SW Poland): Evidence from SHRIMP dating of detrital zircons. Int. J. Earth Sci. 96, 1153–1162.

Lexa, O., Schulmann, K., Janoušek, V., Štípská, P., Guy, a., Racek, M., 2011. Heat sources and trigger mechanisms of exhumation of HP granulites in Variscan orogenic root. J. Metamorph. Geol. 29, 79–102.

Lister, G., Williams, P.F., 1979. Fabric development in shear zones: theoretical controls and observed phenomena. J. Struct. Geol. 1, 283–297.

López-Carmona, A., Abati, J., Pitra, P., Lee, J.K.W., 2014. Retrogressed lawsonite blueschists from the NW Iberian Massif: P-T-t constraints from thermodynamic modelling and 40Ar/39Ar geochronology. Contrib. to Mineral. Petrol. 167, 987.

Machowiak, K., Armstrong, R., 2007. SHRIMP U-Pb zircon age from the Karkonosze granite. Mineral. Pol. Spec. Pap. 31, 193–196.

Maierová, P., Lexa, O., Schulmann, K., Štípská, P., 2014. Contrasting tectono-metamorphic evolution of orogenic lower crust in the Bohemian Massif: A numerical model. Gondwana Res. 25, 509–521.

Malavieille, J., 2010. Impact of erosion, sedimentation, and structural heritage on the structure and kinematics of orogenic wedges: Analog models and case studies. GSA Today 4–10.

Maluski, H., Patočka, F., 1997. Geochemistry and ^{40}Ar-^{39}Ar geochronology of the mafic metavolcanic rocks from the Rychory Mountains complex (west Sudetes, Bohemian Massif): palaeotectonic significance. Geol. Mag. 134, 703–716.

Marheine, D., Kachlík, V., Maluski, H., Patočka, F., Żelazniewicz, A., 2002. The ^{40}Ar/^{39}Ar ages from the West Sudetes (NE Bohemian Massif): constraints on the Variscan polyphase tectonothemal development. In: Winchester, J., Pharaoh, T., Verniers, J. (Eds.), Palaeozoic Amalgamation of Central Europe. Geol. Soc. London Spec. Pub. 201, 133–155.

Matte, P., Maluski, H., Rajlich, P., Franke, W., 1990. Terrane boundaries in the Bohemian Massif: results of large-scale Variscan shearing. Tectonophysics 177, 151–170.

Mazur, S., 1995. Structural and metamorphic evolution of the country rocks at the eastern contact of the Karkonosze granite in the southern Rudawy Janowickie Mts and Lasocki Range (in Polish with English summary). Geol. Sudet. 29, 31–98.

Mazur, S., Aleksandrowski, P., 2001. The Teplá(?)/Saxothuringian suture in the Karkonosze-Izera massif, WesternSudetes, Central European Variscides. Int. J. Earth Sci. 90, 341–360.

Mazur, S., Aleksandrowski, P., Kryza, R., Oberc-Dziedzic, T., 2006. The Variscan Orogen in Poland. Geol. Quart. 50, 89–118.

Mazur, S., Kryza, R., 1996. Superimposed compressional and extensional tectonics in the Karkonosze-Izera Block, NE Bohemian Massif. In: Oncken, O., Jansen, C. (Eds.), Basement Tectonics 11, Europe and Other Regions. Potsdam, Kluwer, Dordrecht, 51–66.

Morales, L.F.G., Casey, M., Lloyd, G.E., Williams, D.M., 2011. Kinematic and temporal relationships between parallel fold hinge lines and stretching lineations: A microstructural and crystallographic preferred orientation approach. Tectonophysics 503, 207–221.

Nahodilová, R., Štípská, P., Powell, R., Košler, J., Racek, M., 2014. High-Ti muscovite as a prograde relict in high pressure granulites with metamorphic Devonian zircon ages (Běstvina granulite body, Bohemian Massif): Consequences for the relamination model of subducted crust. Gondwana Res. 25, 630–648.

Narębski, W., 1994. Lower to Upper Paleozoic tectonomagmatic evolution of NE part of the Bohemian Massif. Zentralbl. Geol. Paläo. I, 961–972.

Nasdala, L., Massonne, H.J. 2000. Microdiamonds from the Saxonian Erzgebirge, Germany: in situ micro-Raman characterisation. Eur. J. Mineral. 12, 495–498.

Newton, R. C., Charlu, T. V., Kleppa, O. J., 1980. Thermochemistry of high structural state plagioclases. Geoch. Cosmoch. Acta 44, 933–941.

Oliver, G.J.H., Corfu, F., Krogh, T.E., 1993. U-Pb ages from SW Poland: evidence for a Caledonian suture zone between Baltica and Gondwana. J. Geol. Soc. London 150, 355–369.

Patočka, F., Fajst, M., Kachlík, V., 2000. Mafic–felsic to mafic–ultramafic Early Palaeozoic magmatism of the West Sudetes (NE Bohemian Massif); the South Krkonoše Complex. Zeitschr. Geol. Wiss. 28, 177–210.

Patočka, F., Pivec, E., Oliveriová, D., 1996. Mineralogy and petrology of mafic blueschists from the Rýchory Mts. crystalline complex (Western Sudetes, Bohemian Massif). Neues Jahrb. Mineral. - Abhandl. 170, 313–330.

Peřestý, V., Lexa, O., Holder, R., Jeřábek, P., Racek, M., Štípská, P., Schulmann, K., Hacker, B.R., subm. Metamorphic inheritance of Rheic passive margin evolution and its early Variscan overprint in the Teplá-Barrandian Unit, Bohemian Massif. J. Metamorph. Geol.

Philippon, M., Gueydan, F., Pitra, P., Brun, J.P., 2013. Preservation of subduction-related prograde deformation in lawsonite pseudomorph-bearing rocks. J. Metamorph. Geol. 31, 571–583.

Pin, C., Majerowicz, A., Wojciechowska, I., 1988. Upper Palaeozoic oceanic crust in the Polish

Sudetes: Nd-Sr isotope and trace element evidence. Lithos 21, 195–209.

Platt, J.P., 1993. Exhumation of high-pressure rocks : a review of concepts of high-pressure Exhumation and processes. Terra Nov. 5, 119–133.

Platt, J.P., 1986. Dynamics Of Orogenic Wedges And The Uplift Of High-Pressure Metamorphic Rocks. Geol. Soc. Am. Bull. 97, 1037–1053.

Plunder, A., Agard, P., Chopin, C., Okay, A.I., 2013. Geodynamics of the Tavşanlı zone, western Turkey: Insights into subduction/obduction processes. Tectonophysics 608, 884–903.

Plunder, A., Agard, P., Chopin, C., Pourteau, A., Okay, A.I., 2015. Accretion, underplating and exhumation along a subduction interface: From subduction initiation to continental subduction (Tavşanlı zone, W. Turkey). Lithos 226, 233–254.

Plunder, A., Agard, P., Dubacq, B., Chopin, C., Bellanger, M., 2012. How continuous and precise is the record of P-T paths? Insights from combined thermobarometry and thermodynamic modelling into subduction dynamics (Schistes Lustrés, W. Alps). J. Metamorph. Geol. 30, 323–346.

Powell, R., Holland, T.J.B., 1999. Relating formulations of the thermodynamics of mineral solid solutions; activity modelling of pyroxenes, amphiboles and micas. Am. Mineral. 84, 1–14.

Rötzler, K., Schumacher, R., Maresch, W.V., Willner, A.P., 1998. Characterisation and geodynamic implications of contrasting metamorphic evolution in juxtaposed high-pressure units of the western Erzgebirge. Eur. J. Mineral. 10, 261–280.

Schmädicke, E., Okrusch, M., Schmidt, W., 1992. Eclogite-facies rocks in the Saxonian Erzgebirge, Germany: high pressure metamorphism under contrasting P-T conditions. Contrib. Mineral. Petrol. 110, 226–241.

Schmid, S.M., Casey, M., 1986. Complete fabric analysis of some commonly observed quartz [c]-axis patterns, in: Hobbs, B.E., Heard, H.C. (Eds.), Mineral and Rock Deformation: Laboratory Studies; the Paterson Volume. American Geophysical Union, Washington DC, pp. 263–286.

Schulmann, K., Kroner, A., Hegner, E., Wendt, I., Konopásek, J., Lexa, O., Štípská, P., Kröner, A., Hegner, E., Wendt, I., Konopásek, J., Lexa, O., Štípská, P., 2005. Chronological constraints on the pre-orogenic history, burial and exhumation of deep-seated rocks along the eastern margin of the Variscan Orogen, Bohemian Massif, Czech Republic. Am. J. Sci. 305, 407–448.

Schulmann, K., Konopásek, J., Janoušek, V., Lexa, O., Lardeaux, J.M., Edel, J.B., Štípská, P., Ulrich, S., 2009. An Andean type Palaeozoic convergence in the Bohemian Massif. Compt. Rendus - Géosci. 341, 266–286.

Schulmann, K., Lexa, O., Janoušek, V., Lardeaux, J.M., Edel, J.B., 2014. Anatomy of a diffuse cryptic suture zone: An example from the Bohemian Massif, European Variscides. Geology 42, 275–278.

Searle, M.P., Warren, C.J., Waters, D.J., Parrish, R.R., 2004. Structural evolution, metamorphism and restoration of the Arabian continental margin, Saih Hatat region, Oman Mountains. J. Struct. Geol. 26, 451–473.

Seston, R., Winchester, J. A., Piasecki, M. A. A., Crowley, Q. G., Floyd, P. A., 2000. A structural model for the western-central Sudetes: a deformed stack of Variscan thrust sheets. J. Geol. Soc. London 157, 1155–1167.

Simpson, C., Schmid, S.M., 1983. An evaluation of criteria to deduce the sense of movement in sheared rocks. Geol. Soc. Am. Bull. 94, 1281–1288.

Skrzypek, E., Štípská, P., Schulmann, K., Lexa, O., Lexová, M., 2011. Prograde and retrograde metamorphic fabrics - a key for understanding burial and exhumation in orogens (Bohemian Massif). J. Metam. Geol. 29, 451–472.

Smulikowski, W., 1995. Evidence of glaucophane-schist facies metamorphism in the East Karkonosze complex, West Sudetes, Poland. Geol. Rundsch. 84, 720–737.

Štědrá, V., Kryza, R., Kachlík, V., 2002. Coronitic metagabbros of the Mariánské Lázně Complex and Teplá Crystalline Unit: inferences for the tectonometamorphic evolution of the western margin of the Teplá-Barrandian Unit, Bohemian Massif. In: Winchester, J.A., Pharaoh, T. C., Verniers, J. (Eds.), Palaeozoic Amalgamation of Central Europe. Geol. Soc. London Spec. Pub. 201, 217–236.

Stipp, M., Stünitz, H., Heilbronner, R., Schmid, S.M., 2002a. The eastern Tonale fault zone: a “natural laboratory” for crystal plastic deformation of quartz over a temperature range from 250 to 700°C. J. Struct. Geol. 24, 1861–1884.

Stipp, M., Stünitz, H., Heilbronner, R., Schmid, S.M., 2002b. Dynamic recrystallization of quartz: correlation between natural and experimental conditions. In: De Meer, S., Drury, M.R., De Bresser, J.H.P., Pennock, G.M. (Eds.), Deformation Mechanisms, Rheology and Tectonics: Current Status and Future Perspectives. Geol. Soc. London Spec. Pub. 200, 171–190.

Štípská, P., Schulmann, K., Kröner, A., 2004. Vertical extrusion and middle crustal spreading of omphacite granulite: a model of syn-convergent exhumation (Bohemian Massif, Czech Republic). J. Metamorph. Geol. 22, 179–198.

Stünitz, H., 1991. Folding and shear deformation in quartzites, inferred from crystallographic preferred orientation and shape fabrics. J. Struct. Geol. 13, 71–86.

Tichomirowa, M., Berger, H.J., Koch, E.A., Belyatski, B.V., Gotze, J., Kempe, U., Nasdala, L., Schaltegger, U., 2001. Zircon ages of high-grade gneisses in the Eastern Erzgebirge (Central European Variscides) – constraints on origin of the rocks and Precambrian to Ordovician magmatic events in the Variscan foldbelt. Lithos 56, 303–332.

Tinkham, D.K., Zuluaga, C.A., Stowell, H.H., 2001. Metapelite phase equilibria modeling in MnNCKFMASH: The effect of variable Al2O3 and MgO/(MgO + FeO) on mineral stability. Geol. Mater. Res. 3, 1–42.

Timmermann, H., Štědrá, V., Gerdes, A., Noble, S.R., Parrish, R.R., Dörr, W., 2004. The problem of dating high-pressure metamorphism: a U-Pb isotope and geochemical study on eclogites and related rocks of the Mariánské Lázně Complex, Czech Republic. J. Petrol. 45, 1311–1338.

Winchester, J.A., Floyd, P.A., Chocyk, M., Horbowy, K., Kozdrój, W., 1995. Geochemistry and tectonic environment of Ordovician meta-igneous rocks in the Rudawy Janowickie Complex, SW Poland. J. Geol. Soc. London 152, 105–115.

Winchester, J. A., Patočka, F., Kachlík, V., Melzer, M., Nawakowski, C., Crowley, Q.G., Floyd, P.A., 2003. Geochemical discrimination of metasedimentary sequences in the Krkonose-Jizera Terrane (West Sudetes, Bohemian Massif): Paleotectonic and stratigraphic constraints. Geol. Carpat. 54, 267–280.

Xypolias, P., Alsop, G.I., 2014. Regional flow perturbation folding within an exhumation channel: A case study from the Cycladic Blueschists. J. Struct. Geol. 62, 141–155.

Xypolias, P., Koukouvelas, I.K., 2001. Kinematic vorticity and strain rate patterns associated with ductile extrusion in the Chelmos Shear Zone (External Hellenides, Greece). Tectonophysics 338, 59–77.

Žák, J., Verner, K., Sláma, J., Kachlík, V., Chlupáčová, M., 2013. Multistage magma emplacement and progressive strain accumulation in the shallow-level Krkonoše-Jizera plutonic complex, Bohemian Massif. Tectonics 32, 1493–1512.

Żelaźniewicz, A., 1997. The Sudetes as a Palaeozoic orogen in central Europe. Geol. Mag. 134, 691–702.

Žáčková, E., Konopásek, J., Jeřábek, P., Finger, F., Košler, J., 2010. Early Carboniferous blueschist-facies metamorphism in metapelites of the West Sudetes (Northern Saxothuringian Domain, Bohemian Massif). J. Metam. Geol. 28, 361–379.

Žáčková, E., Konopásek, J., Košler, J., Jeřábek, P., 2012. Detrital zircon populations in quartzites of the Krkonoše-Jizera Massif – implications for pre-collisional history of the Saxothuringian Domain in the Bohemian Massif. Geol. Mag. 149, 443–458.

Figure and table captions

Fig. 1. (a) Simplified geological map of the northern part of the Bohemian Massif (after Kryza

and Mazur, 1995). The inset in the upper right corner shows the position of the study area with respect to the major Variscan massifs. (b) Simplified geological map of the southern Krkonoše-Jizera Massif (modified after Chaloupský, 1989) showing the location of the studied petrological samples. GPS coordinates of sample EL9/2 and EL217 are 50.6602N, 15.26164E and 50.63941N, 15.84218E ,respectively. Labels (1)–(4) in the legend correspond to the division into four lithological belts as described in the text and shown in Fig. 2b.

Fig. 2. (a) Schematic geometry of the reconstructed mega-scale isoclinal folds F2 refolded by F3. The F2 folds cover the entire studied region as demonstrated by the simplified geological map from Fig. 1b inserted into the present day erosion section in (b). (b) Shows division of the studied area into the three limbs and two hinges of F2 mega-folds. Labels (1)–(4) show the extent of the four major lithological belts winding throughout the studied area: (1) garnet-bearing micaschist, (2) orthogneiss, (3) garnet-free micaschist, phyllite and metavolcanics, and (4) metabasite (cf. Fig. 1b).

Fig. 3. Photographs of observed deformation structures with indicated geographic orientation (AP – axial plane, FA – fold axis). F2 and F3 folds overprinting S1 compositional layering (a) in metabasite near Železný Brod in the eastern part of Limb 3 and (b) in calc-silicates near Velká Úpa near the hinge 1 of the isoclinal mega-fold F2 (Fig. 2). (c) Non-cylindrical folds F2 from the Jeřábník ridge characteristic for the central part of the overturned Limb 2. (d) Photomicrograph and (e) photograph of the isoclinal folds F2 refolded by upright folds F3 in metapelites of Limbs 2 and 3. The subhorizontal axial-planar cleavage S2 is associated with widespread blastesis of albite. (f) Asymmetric folds F3 in orthogneiss from the Labe valley near hinge 1 of the isoclinal mega-fold. (g) Photomicrograph showing the overprint of S2, overgrown by albite porphyroblasts, by subvertical crenulation cleavage S3 in Limb 2. (h) The kink bands F4 affecting S2 foliation and upright folds F3.

Fig. 4. Structural map of the southern Krkonoše-Jizera Massif with simplified geology of Fig. 1b. The map shows the interpolated traces and inclination of the main deformation fabrics S2 and S1, with their L2 and L1 stretching lineation, and fold axial planes AP3 and cleavage S3 with fold axes

FA3.

Fig. 5. Spatial variations in orientation of the main deformation structures across the studied region shown in pole figures 1 – max. 7 associated with regions (dashed line) in the simplified geological map (for map legend see Fig. 4). (a) S1 and S2 foliations (or S2/S1 in most of the area indistinguishable: see text for explanation), (b) L1 and L2 stretching lineations and FA2 fold axes, (c) AP3 fold axial planes and S3 cleavages, and (d) FA3 fold axes. The distribution density function in the pole figures was obtained via the Gaussian counting method (K=100) and the contours are multiples of standard deviation (S). Number of structural measurements (N) and the maximum density distribution contour (e.g. 12S) is indicated in individual pole figures. Crosses in pole figures in (b) correspond to FA2 axes of the isoclinal F2 folds while dots indicate stretching lineation L2 and L1.

Fig. 6. Microstructures of deformed quartz veins and aggregates from the Jizera orthogneiss (cross-polarized lambda plate photographs). (a–c) show microstructures associated with S1 or S2 deformation fabrics characterised by lobate boundaries of recrystallised quartz grains. (b and c) show grain shape preferred orientation inclined with respect to macroscopic foliation suggesting top-to-the WNW shear sensefor S1 in F2 hinge (b) and top-to-the ESE shear sense for S2 in F2 limb. (d) shows an overprint of S1 or S2 microstructure by S3 cleavage and associated microstructure. For location of displayed samples see Fig. 7.

Fig. 7. Crystallographic preferred orientation of recrystallised quartz grains measured by Electron Back Scattered Diffraction (EBSD) in the XZ section of the finite strain ellipsoid from 22 samples distributed along the U-shaped orthogneiss body. Lower hemisphere equal area projection pole figures represent poles to base (0001) [c-axis], poles to the first order prism {10–10} <m-axes> and poles to the second order prism {11–20} <a-axes>. Sample names with Q or G distinction, i.e. quartz veins or orthogneiss samples, respectively, GPS coordinates, dip direction/dip of foliation and stretching lineation, number of measured grains (N) and max of contour diagrams are also indicated. Contours refer to multiples of uniform density distribution. The pole figures are shown in the same

geographic reference frame defined by the approximate east to the right and west to the left of each pole figure, parallel to orientation of the stretching lineation. Note the asymmetric distribution of c-axes and a-axes in several samples used for kinematic interpretation.

Fig. 8. Back-scattered electron images of two orthogneiss and two phyllite samples (for locations see Figs. 7 and 1b, respectively). Orthogneiss samples EL159 (a) and VU88 (b) show replacement of K-feldspar porphyroclasts by albite and phengitic white mica in S1 and S2 fabrics. (b) shows highly phengitic larger flake of white mica related to S1 that is overgrown by smaller flakes of less phengitic white mica related to S2. Phyllite samples EL9/2 (c) and EL217 (d) were used for petrological analysis and P-T estimates. The images in (c) and (d) show the relationship of the peak metamorphic assemblage with respect to S2/S1 foliation.

Fig. 9. The P-T sections calculated in the MnNCKFMASH system for two phyllite samples, EL9/2 (a) and EL217 (b) (see figure 1b for location). The whole rock chemical compositions and compositional isopleths of selected minerals are shown in each P-T section. Within the relatively large stability fields, the resulting P-T estimates were delimited by the isopleths of Si content in phengitic white mica and of X_{Mg} in chlorite and chloritoid.

Fig. 10. A summary P-T diagram showing the peak metamorphic P-T conditions and exhumation P-T path based on the determination of three distinct metamorphic assemblages (M1–M3) and phase equilibrium modelling from several samples presented in this study, in Žáčková et al. (2010) and in Faryad and Kachlík (2013). For localisation of samples see Fig. 1b.

Fig. 11. An evolutionary scheme showing two phases of exhumation of HP rocks in the studied region: (a) via adiabatic exhumation and cold underplating, relamination, in the subduction channel (M1 to M2) and (b) via collisional forced folding due to shortening in the accretionary wedge at the late stages of convergence (M2 to M3).

Table 1. Representative microprobe analyses of selected minerals.

*Figure
Click here to download high resolution image

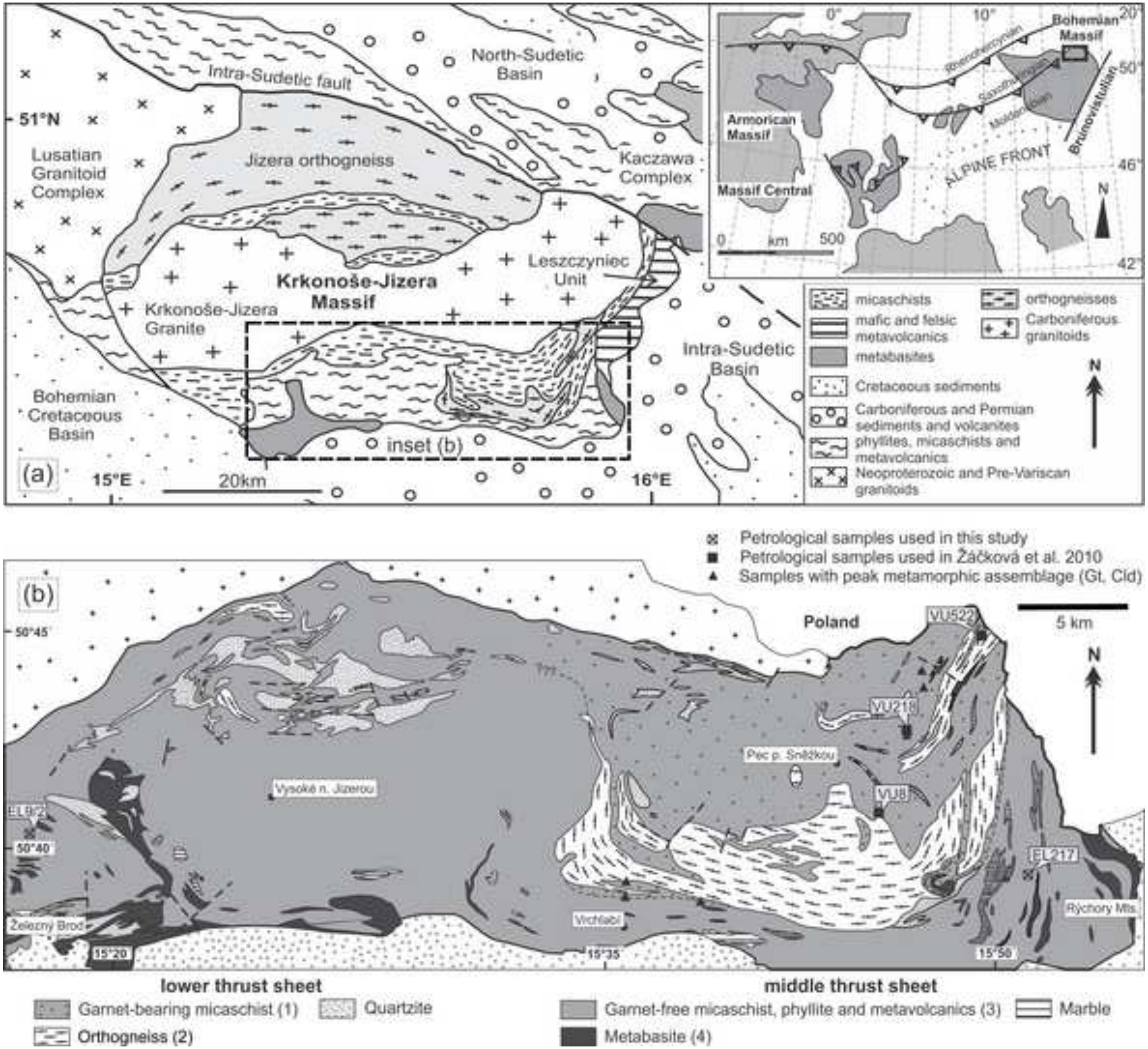

*Figure
Click here to download high resolution image

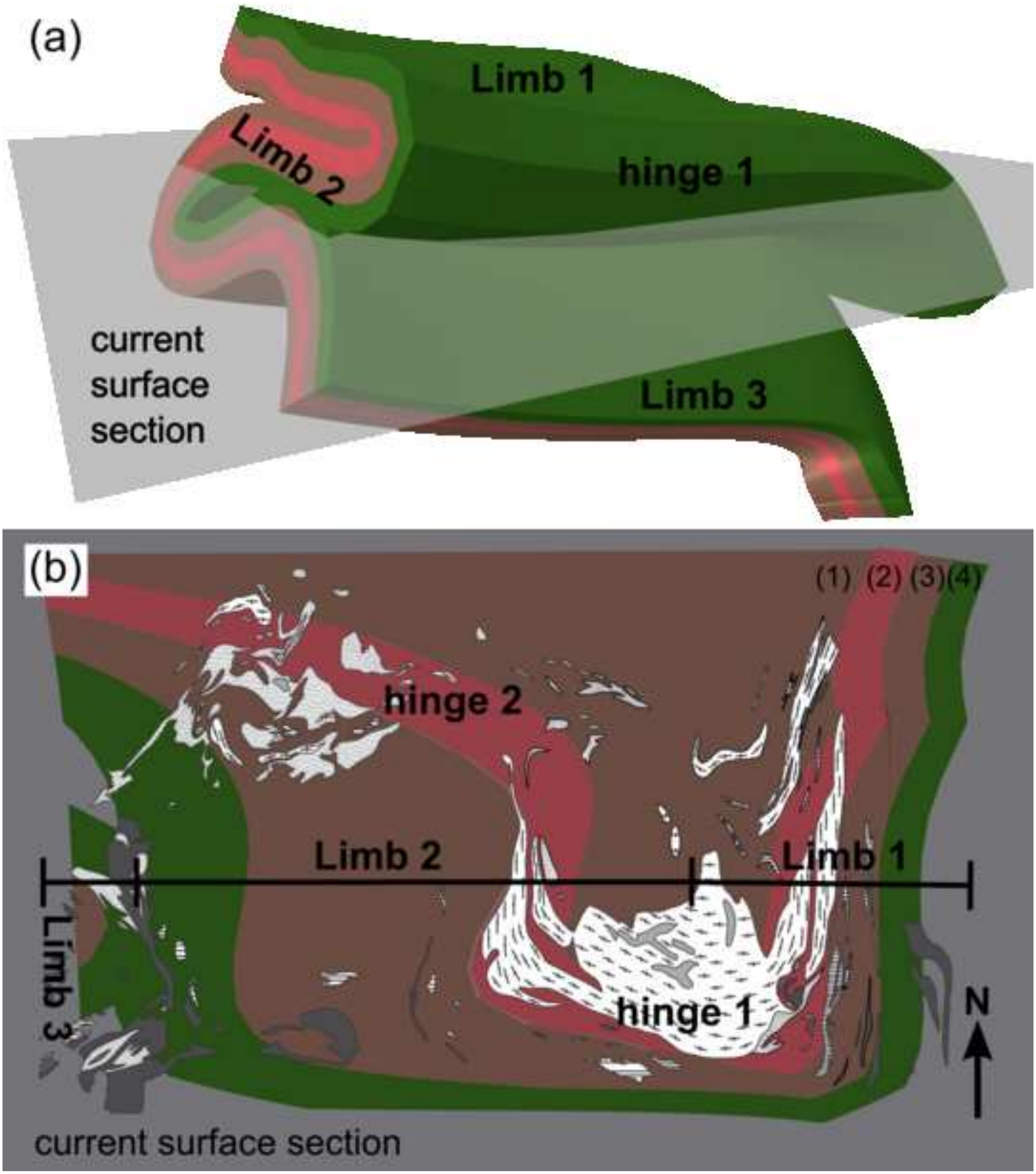

*Figure
Click here to download high resolution image

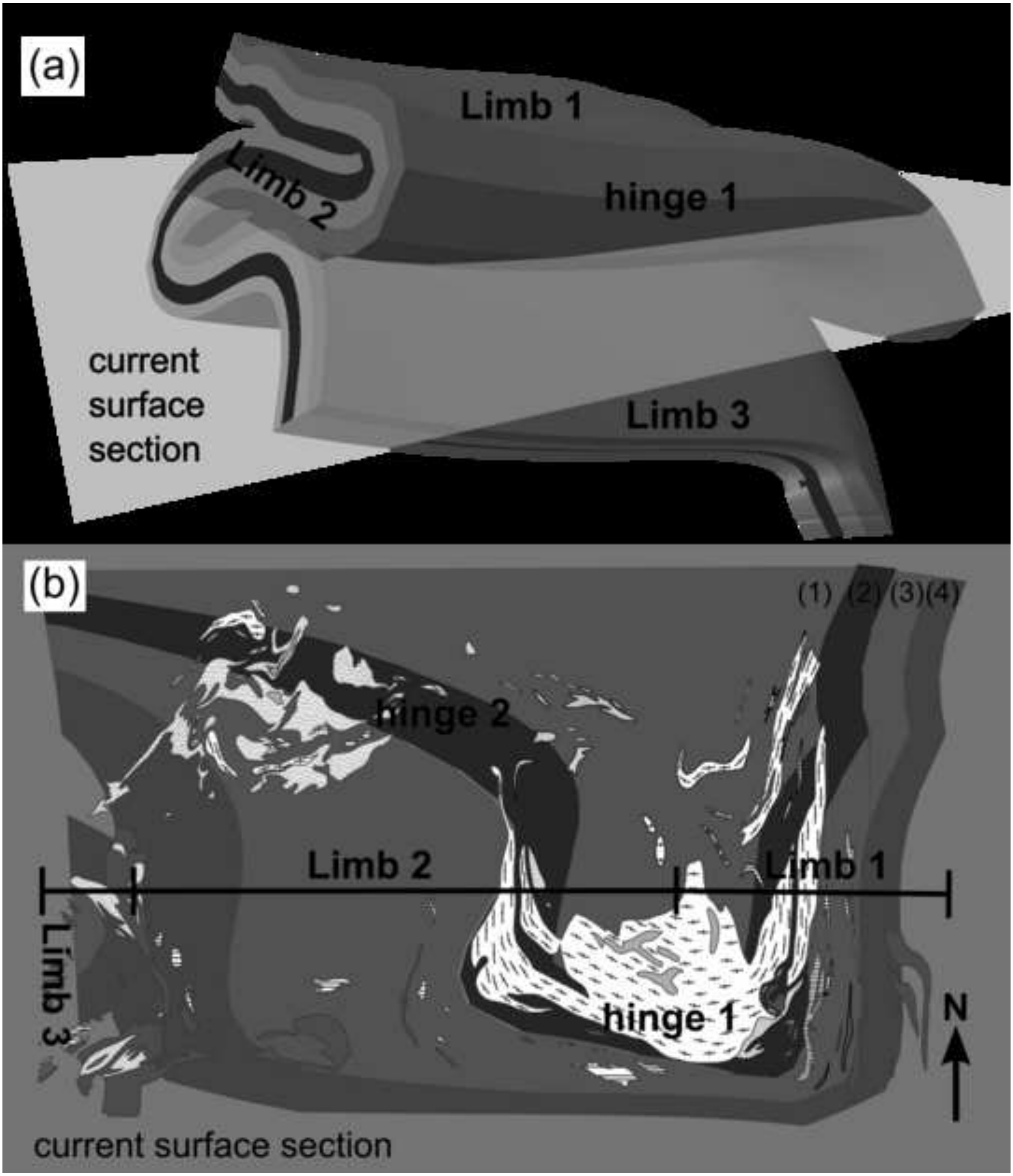

***Figure**

Click here to download high resolution image

*Figure
Click here to download high resolution image

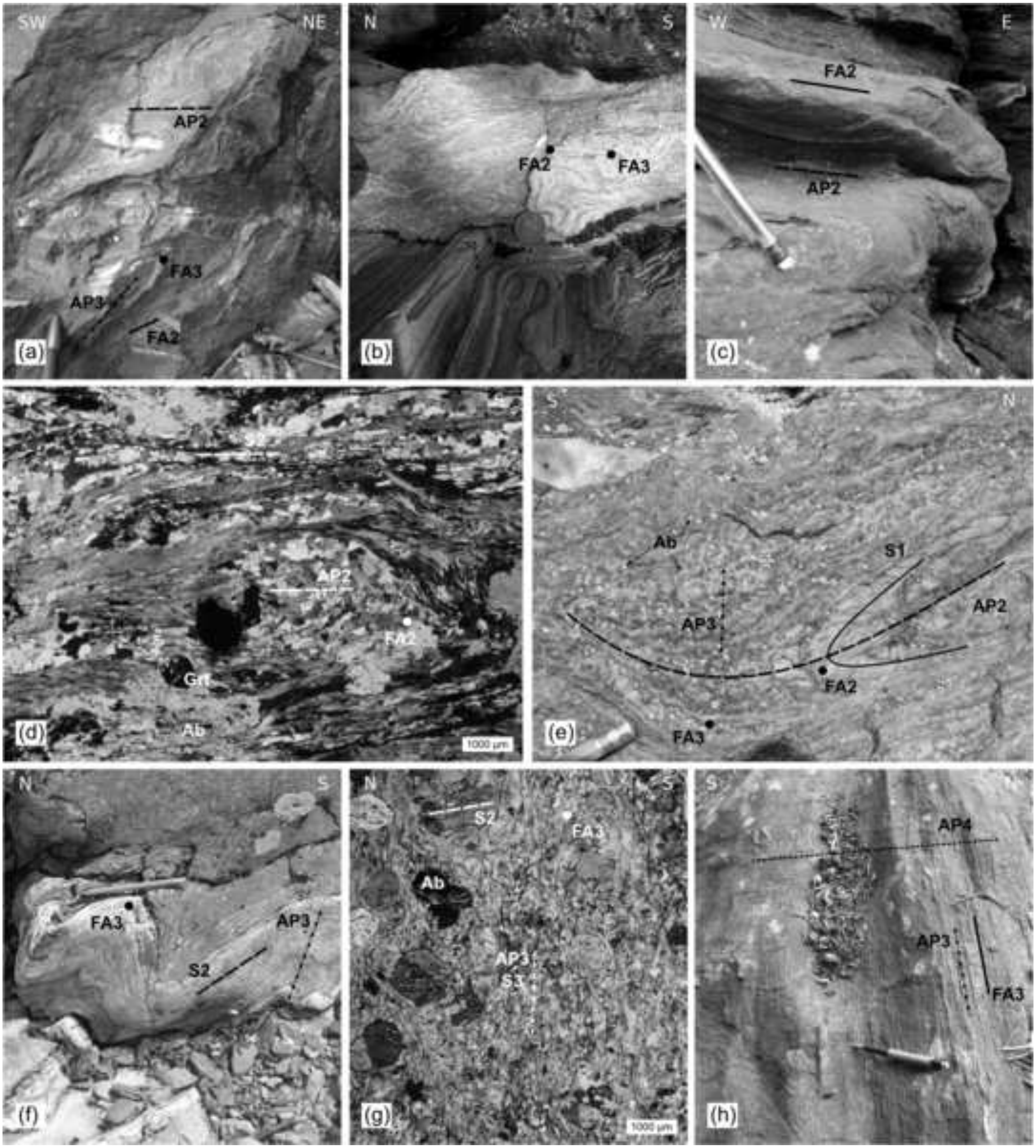

*Figure
Click here to download high resolution image

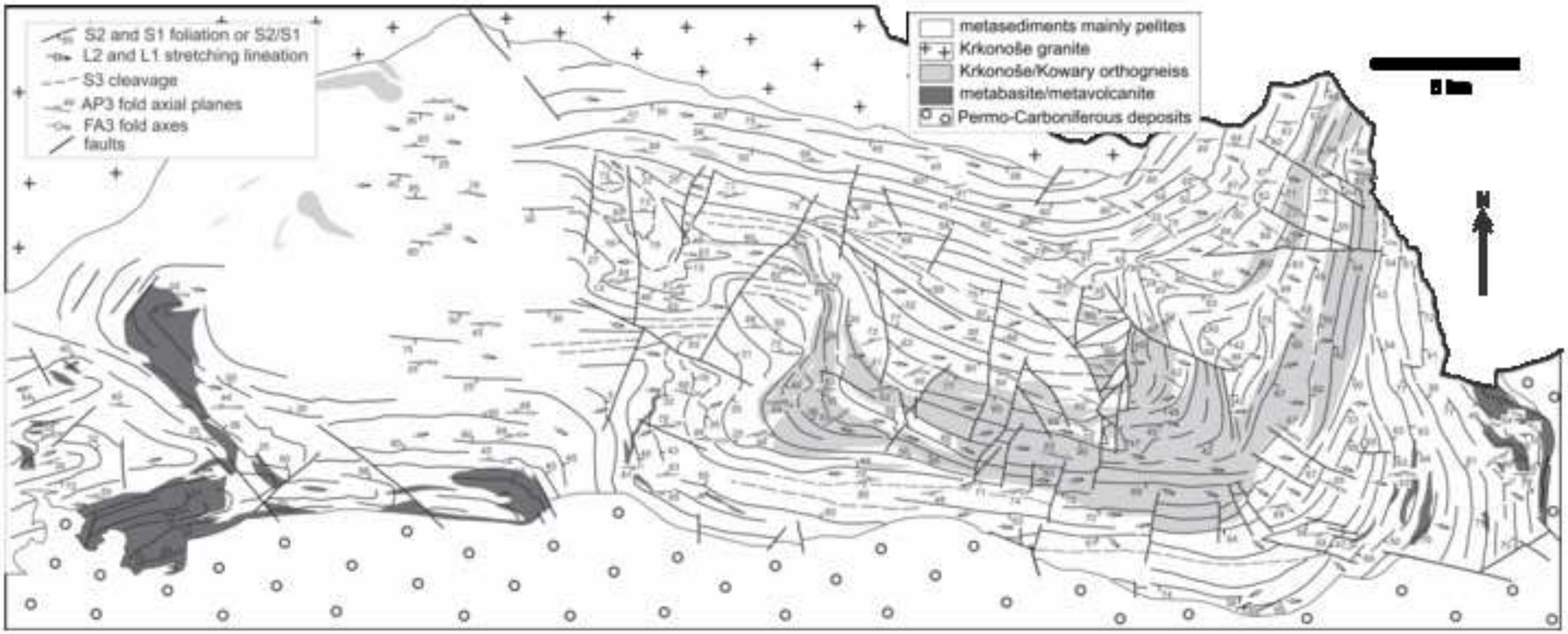

*Figure
Click here to download high resolution image

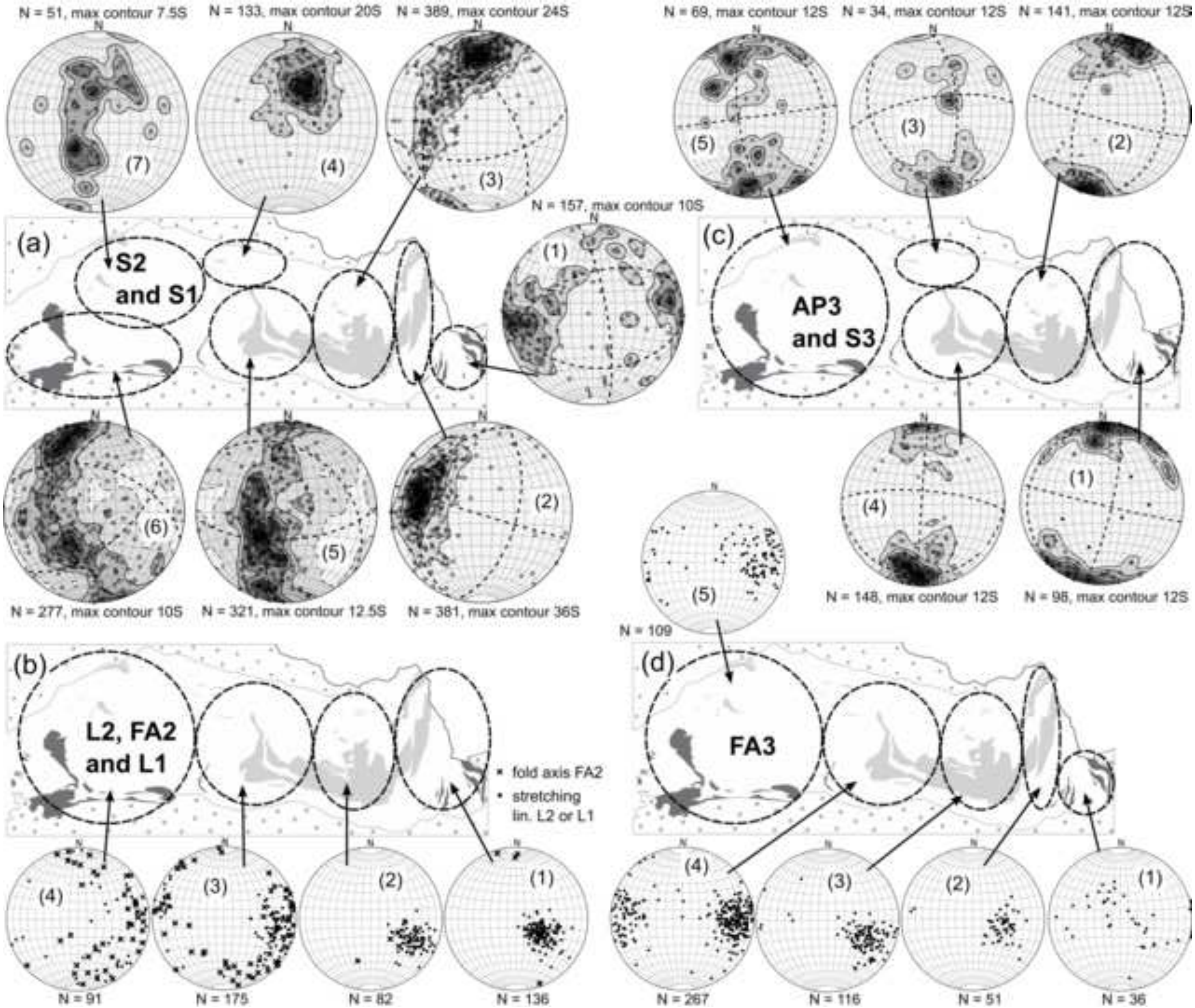

*Figure
Click here to download high resolution image

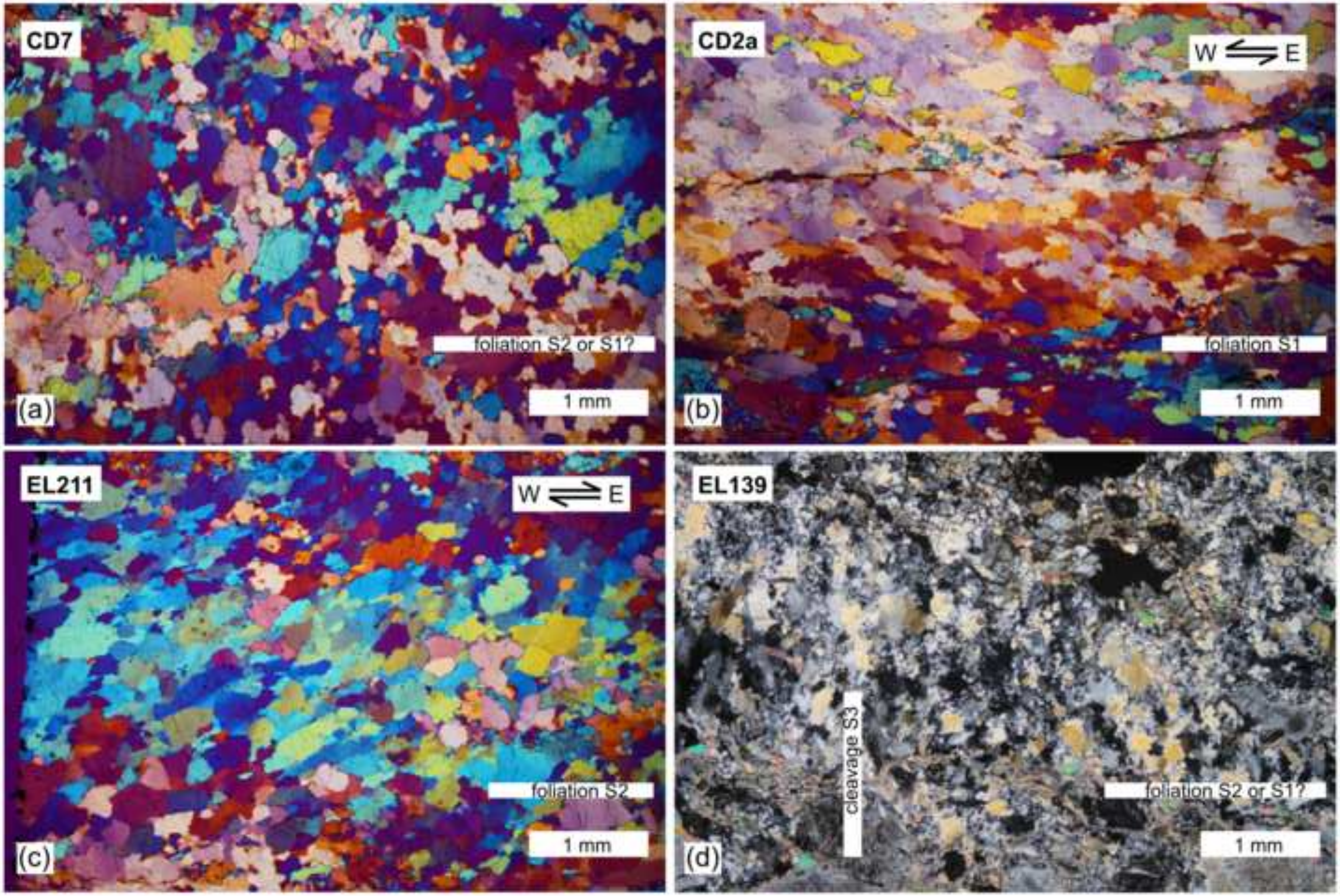

*Figure
Click here to download high resolution image

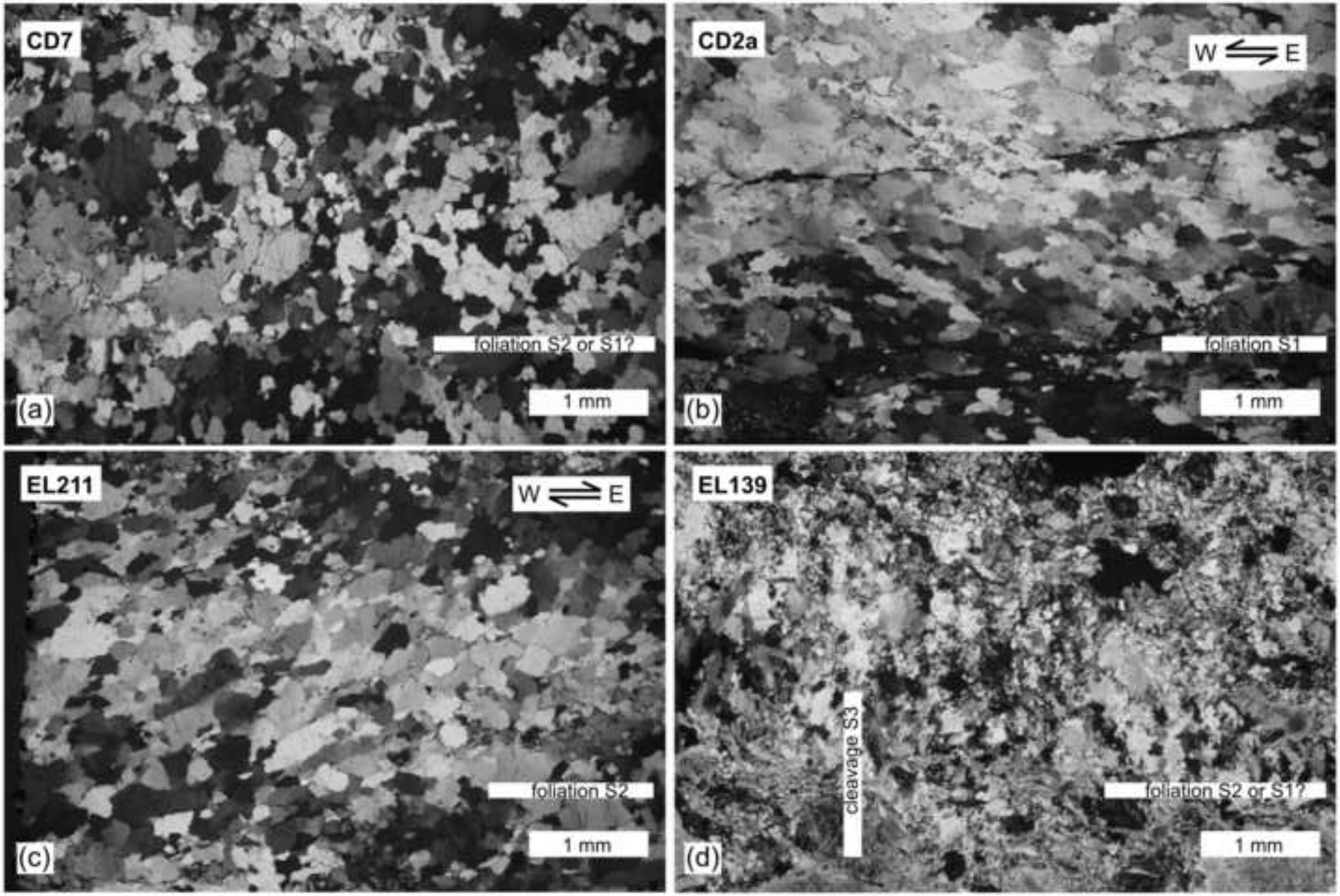

*Figure

Click here to download high resolution image

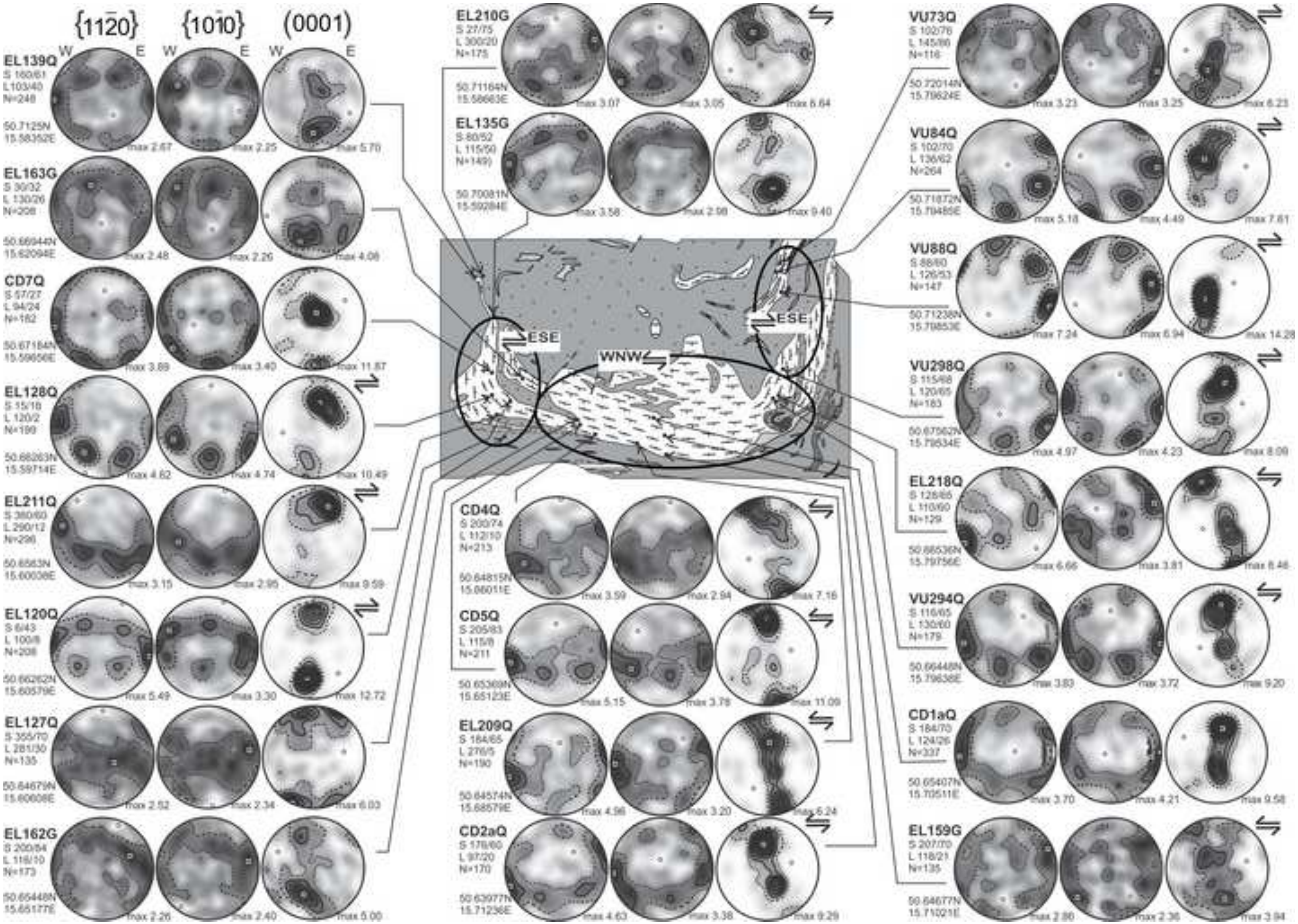

*Figure
Click here to download high resolution image

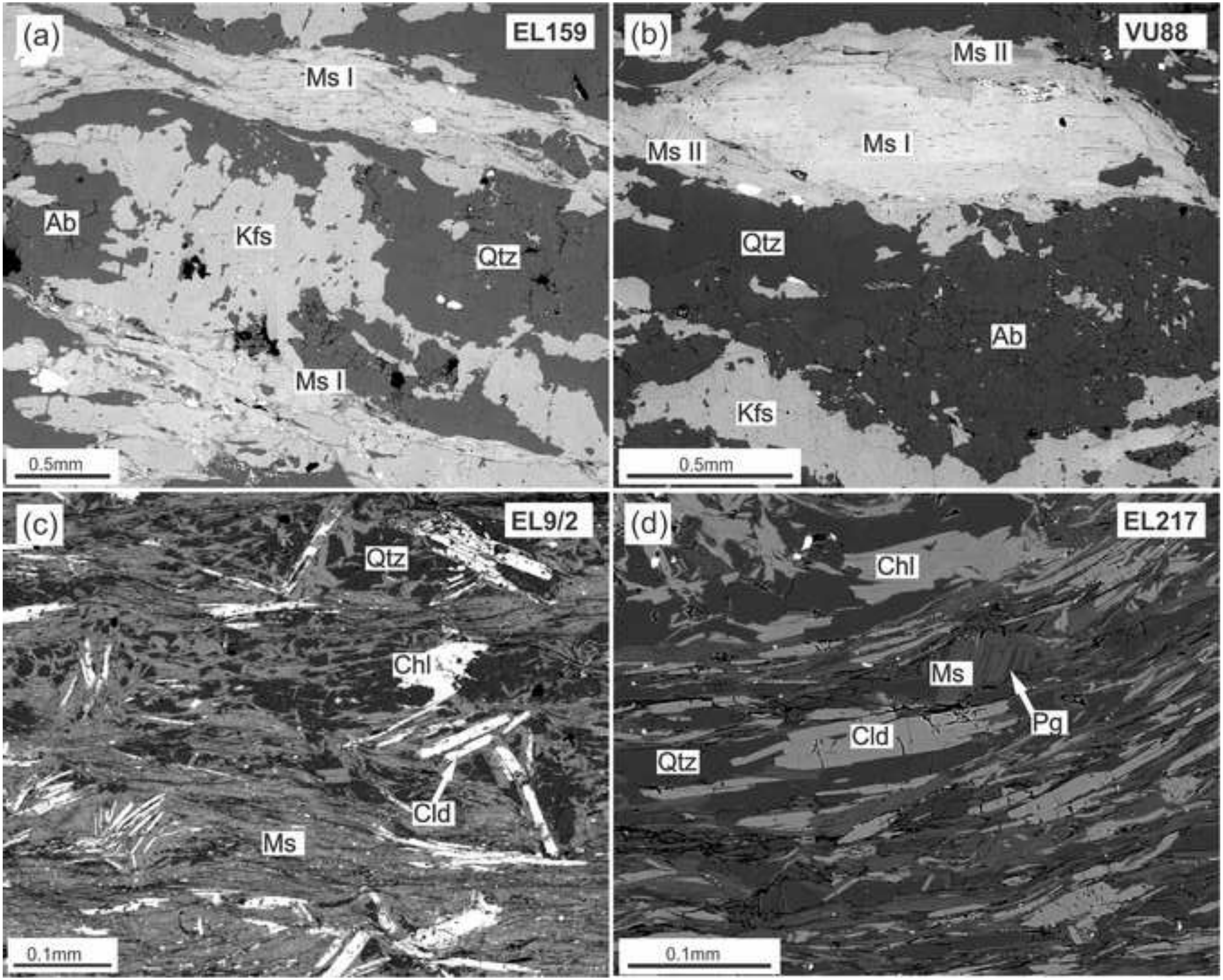

*Figure
Click here to download high resolution image

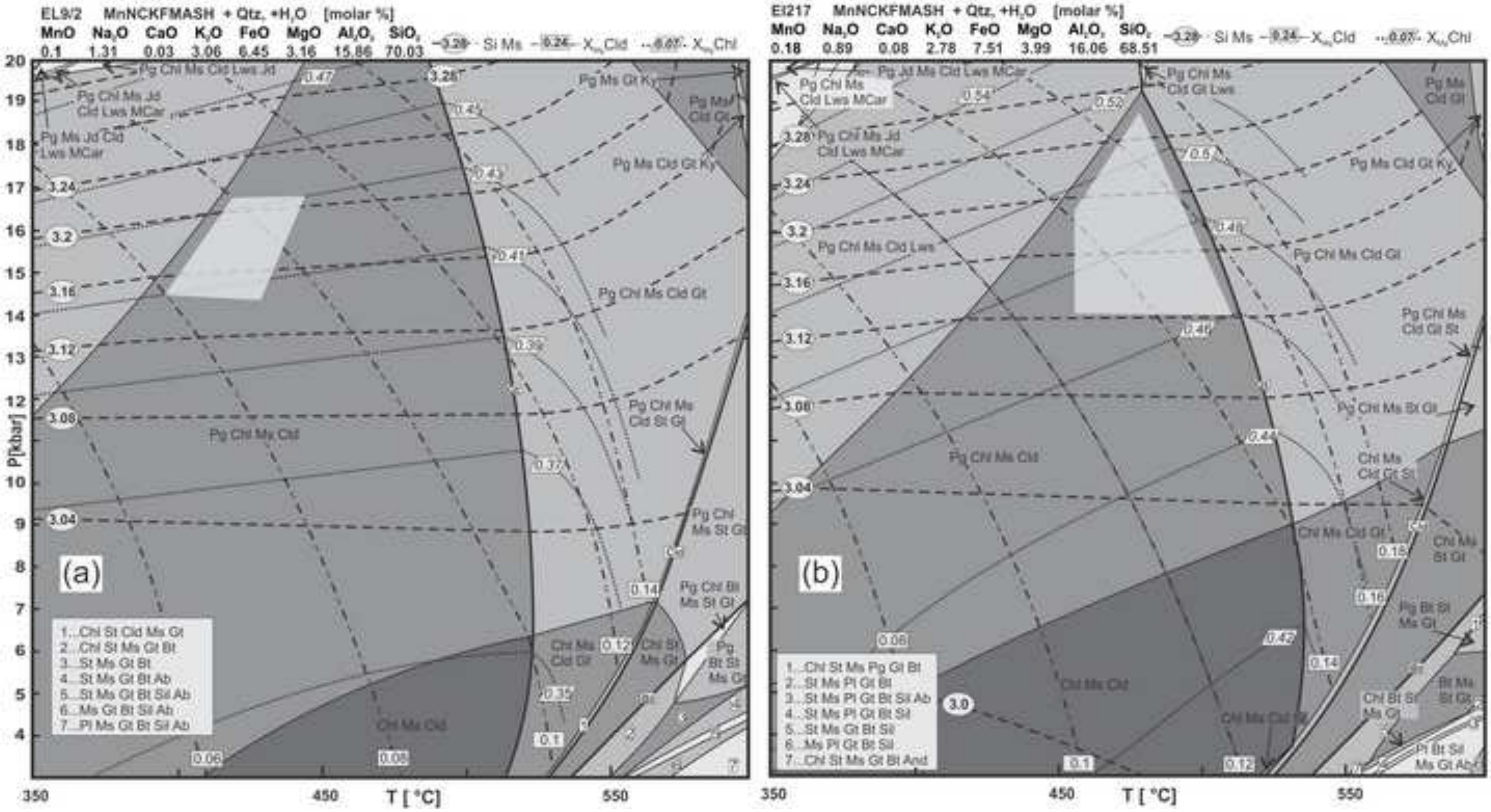

*Figure
Click here to download high resolution image

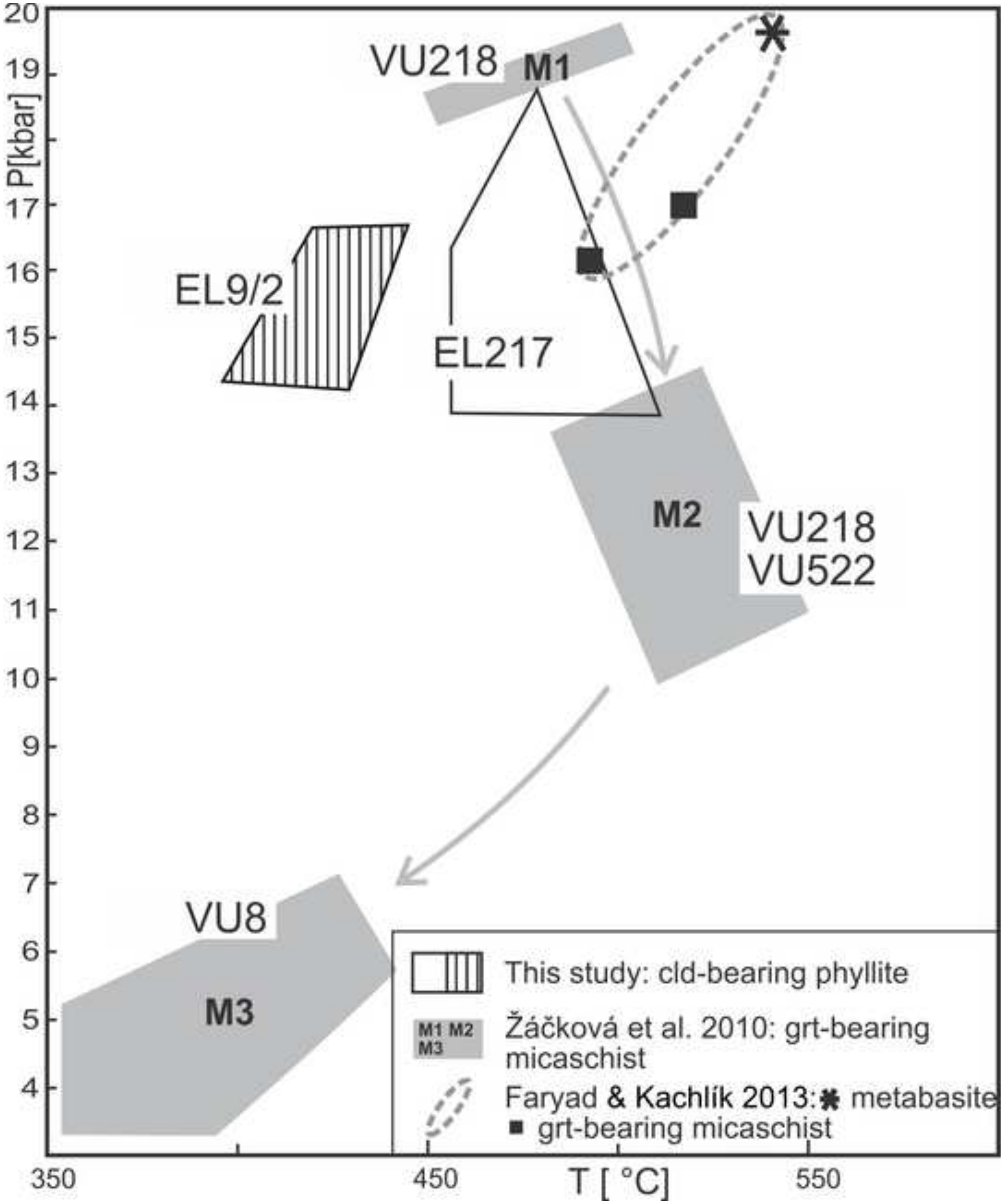

*Figure
Click here to download high resolution image

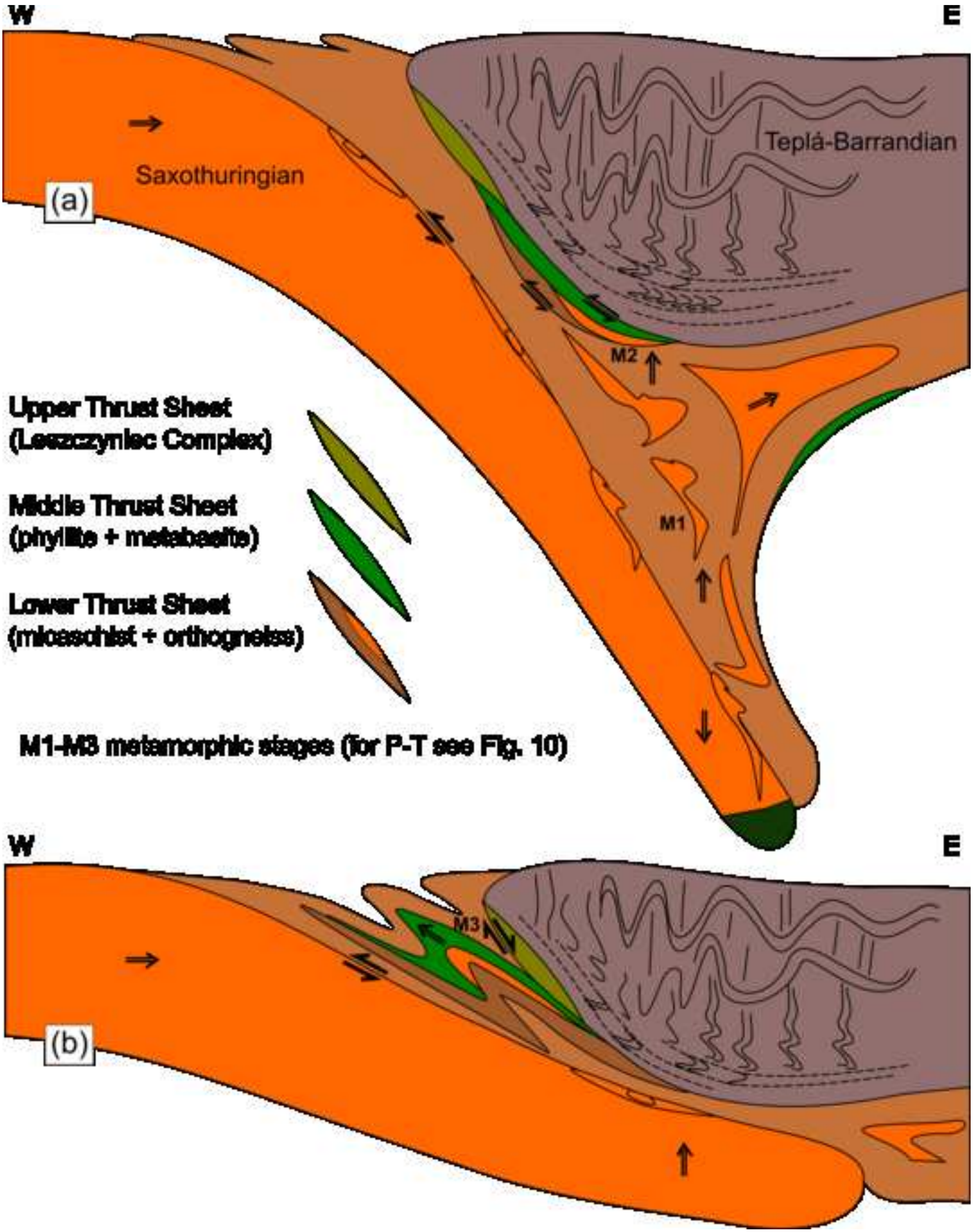

*Figure
Click here to download high resolution image

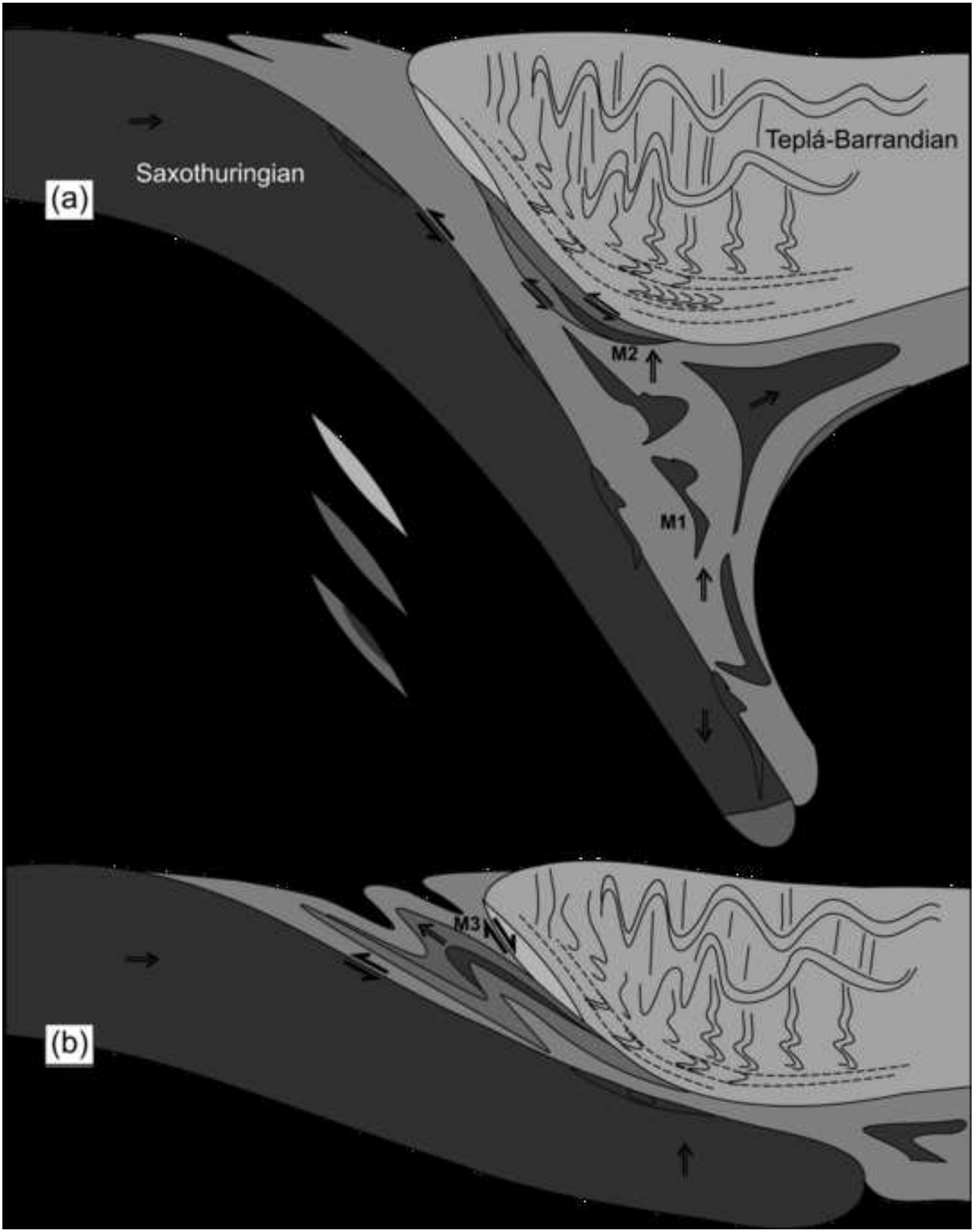

Table

Table 1. Representative microprobe analyses of minerals

Rock	orthogneiss			phyllite					
Sample	EL159	VU88	VU88	EL217	EL217	EL217	EL9/2	EL9/2	EL9/2
Mineral	Ms I	Ms I	Ms II	Cld	Ms	Chl	Cld	Ms	Chl
Wt%									
SiO2	50.39	49.61	46.36	25.19	48.99	26.73	24.65	47.33	24.17
TiO2	0.13	0.10	0.27	0.03	0.10	0.04	0.07	0.11	0.02
Cr2O3	0.00	0.00	0.00	0.02	0.02	0.01	0.03	0.01	0.03
Al2O3	24.23	23.92	28.07	40.33	32.26	20.87	39.66	33.19	23.56
FeO	6.89	8.57	6.50	23.92	1.51	26.05	26.53	3.00	29.74
MnO	0.09	0.11	0.12	0.63	0.00	0.32	0.92	0.03	0.35
MgO	1.09	0.89	0.73	2.37	1.63	14.21	1.31	0.72	9.22
CaO	0.00	0.00	0.00	0.01	0.00	0.00	0.00	0.02	0.03
Na2O	0.03	0.05	0.17	0.00	0.50	0.00	0.01	0.95	0.03
K2O	11.23	11.28	11.12	0.03	9.75	0.00	0.00	9.32	0.02
F	0.33	1.04	0.73	0.01	0.32	0.09	0.00	0.00	0.00
Cl	0.00	0.00	0.00	0.02	0.02	0.01	0.00	0.00	0.00
Total	94.09	94.54	93.35	92.56	95.11	88.33	93.17	94.68	87.16
#O									
Si	3.50	3.44	3.22	2.06	3.24	5.58	2.04	3.17	5.24
Ti	0.01	0.01	0.01	0.00	0.01	0.01	0.00	0.01	0.00
Cr	0.00	0.00	0.00	0.00	0.00	0.00	0.00	0.00	0.01
Al	1.98	1.96	2.30	3.89	2.51	5.14	3.86	2.62	6.02
Fe3+	0.01	0.16	0.24	0.11	0.03	0.00	0.13	0.00	0.00
Fe2+	0.39	0.34	0.13	1.53	0.05	4.55	1.70	0.17	5.40
Mn	0.01	0.01	0.01	0.04	0.00	0.06	0.06	0.00	0.06
Mg	0.11	0.09	0.08	0.29	0.16	4.42	0.16	0.07	2.98
Ca	0.00	0.00	0.00	0.00	0.00	0.00	0.00	0.00	0.00
Na	0.00	0.01	0.02	0.00	0.06	0.00	0.00	0.12	0.00
K	0.99	1.00	0.99	0.00	0.82	0.00	0.00	0.80	0.00
F	0.07	0.23	0.16	0.00	0.00	0.06	0.00	0.00	0.00
Cl	0.00	0.00	0.00	0.00	0.00	0.00	0.00	0.00	0.00
Sum	7.00	7.00	7.00	8.00	7.00	20.00	8.00	7.00	20.00
XMg				0.16		0.49	0.08		0.36